Politecnico di Torino

Corso di Laurea Magistrale
Ingegneria Energetica e Nucleare

A.a. 2023/2024
Sessione di Laurea Marzo 2024

Array Design and Levelized Cost of Energy of Wave Energy Farm

Relators:
Prof. Giuseppe Giorgi
Dr. Emilio Faraggiana
Ing. Cervelli Giulia

Candidate:
Shi Yuwei

ACKNOWLEDGEMENT

I would like to express my sincere gratitude to Professor Giorgi for his trust and for providing me with the opportunity to conduct research in wave energy. His guidance and explanations have been invaluable in shaping my understanding of the subject.

I am also grateful to Dr. Faraggiana for his thoughtful guidance during this journey and Ing. Cervelli for her assistance on the MORE-EST Platform.

To my family, T.L., and friends, I sincerely appreciate your unwavering support. Your companionship has been instrumental in my academic journey.

•

SUMMARY

This thesis aims to contribute to advancing and commercialising wave energy technology by developing a wave energy array design tool based on the MORE-EST Platform from the MOREnergy lab. It begins with exploring current energy policies and renewable energy scenarios in the EU, focusing on the wave energy Levelized Cost of Energy target outlined in The European Strategic Energy Technology Plan.

Chapter 2 lays the foundation by introducing the mathematical models crucial to the design tool, including linear wave theory, point absorber mathematical model, etc. Chapters 3 to 5 detail the tool's development process and its application in simulating a wave energy converter farm project in the oceans surrounding Italy.

The development process encompasses project site selection, array generation, and array configuration optimisation. Site selection involves the consideration of three categories of criteria: Restrictive Sector, Economic Sector, and Technical Sector criteria. Array generation allows users to input array parameters to create arrays at selected sites. Array configuration optimisation utilises technical and economic models to evaluate array configurations' technical performance and economic viability, aiming to identify optimal configurations under specific wave conditions and WEC parameters.

The simulated wave energy converter farm is located west of Sicily, generating single-row, two-row, and three-row arrays comprising 10 WECs. Configuration optimisation is conducted for these arrays, with the rhombus configuration emerging as a relatively superior structure for head sea conditions.

Overall, this thesis presents a comprehensive approach to wave energy array design, offering insights into the technical and economic assessment influencing optimal array configurations and hoping to contribute to the potential commercialisation of wave energy fields.

TABLE OF CONTENTS

LIST OF TABLES

LIST OF FIGURES

ACRONYMS

Acronym	Abbreviation
WEC	Wave Energy Converter
swh	Significant Wave Height
mwp	Mean Wave Period
mwd	Mean Wave Direction
LCoE	Levelized Cost of Energy
CAPEX	Capital Expenditures
OPEX	Operating Expense
AEP	Annual Energy Production
GHG	Greenhouse Gas
SET Plan	The European Strategic Energy Technology Plan
PTO	Power Take-Off
BEM	Boundary Element Method
MVI	Monthly Variation Index

Chapter: 1 Introduction

1.1 Energy Policies

European renewable energy policy was initiated with the publication of the White Paper (Energy for the Future: Renewable Energy Sources) [1]. As the 21st century progressed, the implications of climate change increasingly influenced European energy policy. The European Union has been dedicated to creating a robust policy framework and establishing legally binding targets for sustainable energy development, facilitating the energy sector's transition.

In 2007, the European Council adopted the "2020 Climate and Energy Package," which aimed to reduce EU GHG emissions by 20% relative to 1990 levels, elevate the share of renewable energy in EU energy to 20%, and enhance energy efficiency by 20%.[2] The "2030 Climate and Energy Framework" was subsequently endorsed by the European Council in 2014, setting preliminary targets for the EU's climate and energy development by 2030, including a reduction in GHG emissions by 40% compared to 1990 levels, an increase in the share of renewable energy in EU energy to 27%, and an improvement in energy efficiency by 27%.[3] The goal of reducing GHG emissions by 40% subsequently served as the foundation for the EU's Nationally Determined Contribution (NDC) under the framework of the Paris Agreement.[4]

In 2018, the European Union revised the Renewable Energy Directive (RED) and the Energy Efficiency Directive (EED), setting forth objectives to raise the share of renewable energy in EU energy to 32% and increase energy efficiency by 32.5% by 2030.

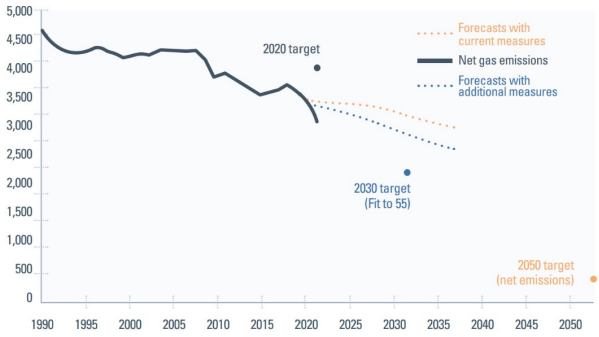

Figure 1.1 Evolution of Greenhouse Gas Emissions in EU (Model: MTCO2E)[5]

Then, the "The European Green Deal " was ratified by the European Commission in 2020, delineating a strategic roadmap for a transition towards a carbon-neutral circular economy [6]. This plan included the "Fit for 55 in 2030" package, which augmented the target for GHG reduction in 2030 to 55% and set a goal for achieving climate neutrality by 2050. [7] In 2022, the European Commission further amended the Renewable Energy Directive (RED) in response to the Russia-Ukraine conflict and the ensuing energy security crisis. This amendment increased the share of the renewable energy target for 2030 to 45%, which is anticipated to elevate the total renewable energy generation capacity to 1236 GW by 2030. [8]

1.2 Renewable Energy and Offshore Energy

To address the ambitious goals of reducing greenhouse gas emissions and increasing renewable energy adoption, the European Union (EU) is undergoing a transformative shift in its energy system. This shift involves gradually reducing carbon emissions from energy production and consumption to establish a low-carbon or carbon-neutral energy system. Central to this transformation is the enhancement of energy efficiency and the expansion of renewable energy sources.

Since 2010, the dividends brought forth by the rapid development of offshore wind energy underscored the considerable potential and efficiency of offshore renewable energy relative to onshore sources to stakeholders and government.

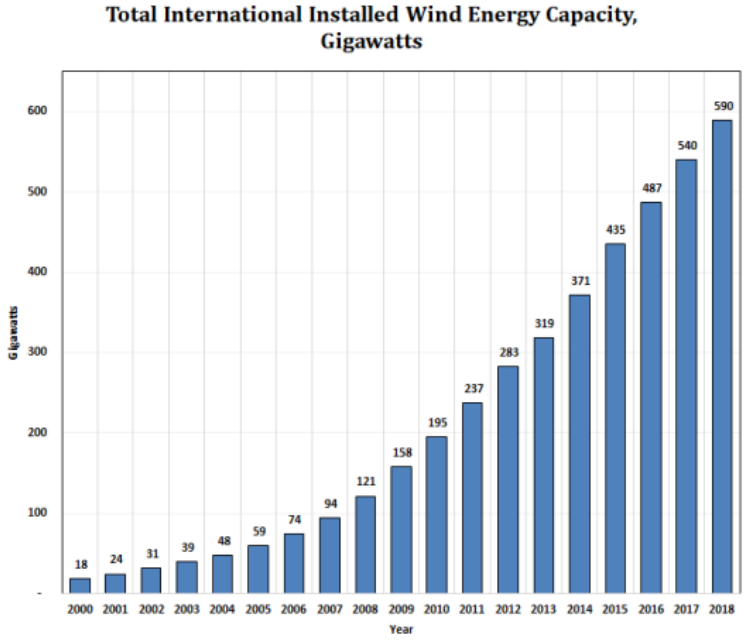

Figure 1.2 Global Wind Energy Capacity Growth. [9]

To ensure that offshore renewable energy can help reach the EU's ambitious energy and climate targets, the Commission introduced a dedicated EU strategy on offshore renewable energy (COM (2020)741) in November 2020. This strategy outlines targets for offshore wind and ocean energy, aiming for an installed capacity of at least 60 GW of offshore wind and 1 GW of ocean energy by 2030 and 300 GW and 40 GW, respectively, by 2050.

Ocean energy, comprising wave, tidal technologies, and so on, holds immense promise in supporting the EU's climate objectives while leveraging a robust European

supply chain connected to various industries. Over the past decade, the EU and private sector have invested significantly, with more than €4 billion allocated to ocean energy research and pilot projects. The European Strategic Energy Technology Plan (SET Plan) further underscores the importance of ocean energy, setting ambitious cost-reduction targets for tidal and wave technologies. By aiming for more competitive pricing, with targets of 200 EUR/MWh by 2025 and 150 EUR/MWh by 2030, the SET Plan seeks to drive innovation and accelerate the deployment of ocean energy technologies across Europe. [10]

1.3 Wave Energy Technologies

Ocean energy encompasses diverse technologies, including wave energy, tidal Stream Energy, tidal range energy, ocean thermal energy conversion (OTEC), and salinity gradient power generation. This variety offers the European Union a significant opportunity to shift towards a more sustainable and renewable energy infrastructure, potentially fulfilling 10% of its current power demand by 2050, which aligns with the EU's ambitious objective to significantly decrease GHG emissions, expanding its energy portfolio beyond solar and wind sources.

Among these ocean energy technologies, wave energy and tidal Stream Energy stand out for their market potential and scalability within Europe. The global theoretical resource for wave energy alone is estimated at $29,500$ TWh/year [11], more than humanity's total annual electrical energy consumption [12]. These immense potential positions wave energy as a crucial component in the EU's renewable energy mix.

Figure 1.3 Wave

Wave Energy Converter is a device that harnesses and transforms the kinetic energy of the waves into electrical power. These devices include point absorbers, attenuators, oscillating water columns, overtopping devices, submerged pressure differentials, and rotating mass devices.

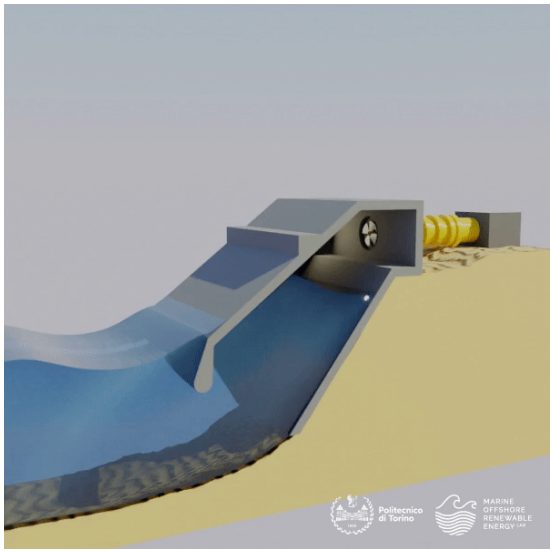

Figure 1.4 Oscillating Water Column

The Oscillating Water Column is a unique wave power extraction technology that can be located onshore or in deeper water offshore. It is characterised by the presence of an air chamber. The air chamber can harness wave power and convert it to pneumatic power, and a PTO system can transform this pneumatic power into electricity.

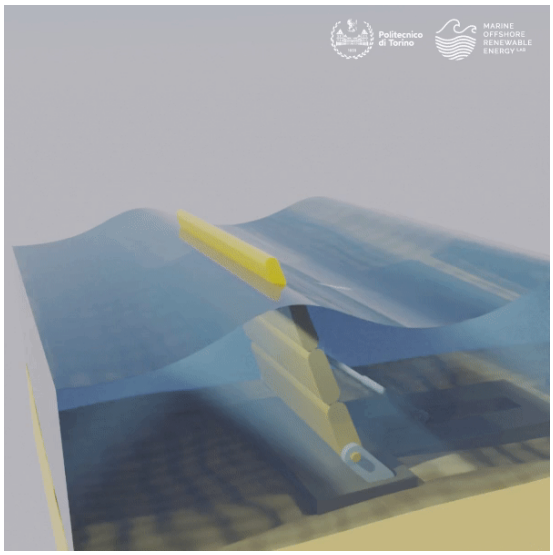

Figure 1.5 Oscillating Wave Energy Converter

Oscillating Wave Energy Converters feature a design with a fixed base anchored to the seabed and a movable part linked to this base. It can capture energy from the relative movement of the oscillating part as waves pass, moving water particles along with it.

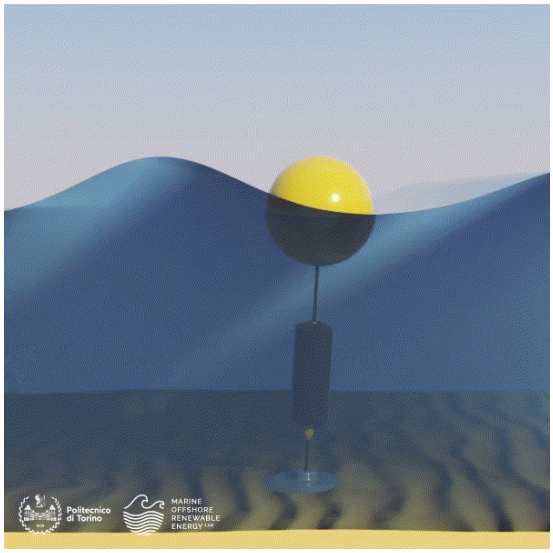

Figure 1.6 Point Absorber

Point absorbers usually consist of a floating or submerged buoy that extracts the wave energy with a PTO system from the relative motion between the wave-activated, moving buoy and a fixed reference.

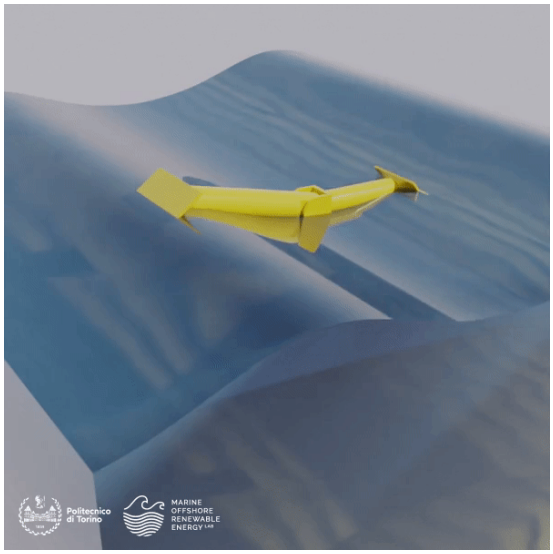

Figure 1.7 Surface attenuator

Surface attenuators consist of several linked segments that align with the direction of incoming waves. The movement of the waves causes the attenuator to flex, converting the kinetic energy of the waves into mechanical energy. This energy can then be converted into electricity through rotational motion or driving hydraulic pumps.

Others like overtopping devices that capture sea water of incident waves in a reservoir above the sea level, then release the water back to sea through turbines and [13] generate electricity.

1.4 Development and Deployment in EU

Over recent years, significant progress has been made in developing and deploying Wave Energy Converters, [14] with the Mediterranean region showing particular promise due to its expansive coastlines.

The inaugural deployment of an off-grid WEC was by Eco Wave Power at Jaffa Port, Israel, in 2014, utilising point absorber technology [15]. The following year saw the deployment of H24 by 40South Energy Italia Srl in Marina di Pisa, Italy, which later connected to the national grid, marking it as a significant nearshore test WEC project in the Mediterranean. [16]

At the same time, the University of Campania Luigi Vanvitelli introduced an overtopping WEC: Overtopping Breakwater for Energy Conversion at Naples Port, Italy, for energy generation and port protection. [17]

Subsequent years saw further installations, including the Inertial Sea Wave Energy Converter off Pantelleria Island by the Politecnico di Torino and Wave for Energy Srl, and the deployment of 100 kW WECs by Eco Wave Power in Gibraltar, also integrated with the photovoltaic panels to test the possibility of photovoltaic panels installation in their future WECs. [18]

Figure 18 Inertial Sea Wave Energy Converter from PoliTO

The largest wave power project in the Mediterranean to date is situated in Civitavecchia Port, featuring a 2500 kW installation by the Mediterranean University of Reggio Calabria and Wavenergy. It incorporates the REWEC3 into the port's breakwater. [19]

In 2018, Ocean Power Technologies deployed Eni's PB3 PowerBuoy WEC off Ravenna, Italy, to demonstrate WEC applicability in oil and gas operations, with a power output of 3 kW and dual functionality in energy and communication. [20]

1.5 The Objective and Outline of Thesis

Objective:

The objective of this thesis is to develop a wave energy array design tool, utilising the MORE-EST Platform from MOREnergy lab, aimed at facilitating the commercialisation of wave energy fields. By exploring current energy policies and renewable energy scenarios and focusing on achieving the wave energy LCoE target set forth by the SET Plan, this thesis seeks to elucidate the development process of the design tool and simulate a WEC farm project via it. By introducing and incorporating site selection criteria and mathematical models relevant to the tool, including linear wave theory, point absorber mathematical models, and so on, the thesis aims to provide a basic framework for optimising wave energy array configurations. The primary objective is to simulate a WEC array project in the oceans surrounding Italy, utilising the developed tool to conduct site selection, array generation, and array configuration optimisation. Through this process, the thesis aims to identify optimal configurations under specific wave conditions and WEC parameters, with the goal of contributing to a bit of advancement and commercialisation of wave energy technology.

Outline:

Chapter 2

This chapter introduces linear wave theory, the mathematical model for Point Absorbers, and the technical and economic models. Linear wave theory is the foundational theory this thesis builds, and several formulas within the technical model are derived from it.

Chapter 3

This chapter will provide an overview of metocean-related databases, as waves serve as the primary "fuel" for WEC devices. Following this, the criteria and thresholds for the site selection process will be outlined. The results of the site selection process will then be presented, along with a sensitivity analysis to identify the most crucial criteria. The work in this chapter has been carried out using QGIS and Python.

Chapter 4

Chapter: 1 Introduction

This chapter will detail the methodology for calculating the AEP of individual WEC devices. Additionally, it will introduce a method for arranging WEC arrays within a selected area based on input parameters and automatically rotating them to meet the mwd requirement. The work in this chapter has been conducted using QGIS and Python.

Chapter 5

In this chapter, the optimisation process for array configuration will be discussed. There are two optimisation directions: one focusing on technical aspects, specifically the q factor or the AEP of the array, and the other on techno-economic considerations, with LCoE serving as the quantification metric in this study. Additionally, this chapter will consider the impact of wave number k on array configuration optimisation. The work in this chapter has been carried out mainly using Python.

Chapter: 2 Mathematical Model

2.1 Linear Wave Theory

In ocean waves, linear wave theory is often used to study surface gravity waves propagating along the interface between water and air. These waves are typically described using the Airy wave theory, a linear wave theory that assumes idealised conditions, such as deep water and no dissipation. Airy wave theory provides solutions for wave height, wave speed, and other wave properties based on linear wave theory principles.

The core of linear wave theory lies in its description of the behaviour of small amplitude waves within a fluid medium, predicated on the assumption that the wave height is negligible compared to the wavelength. Several vital characteristics underpin this theory:

(a) Assumptions: Central to linear wave theory is the assumption of an inviscid and incompressible fluid medium. Additionally, it presupposes a sinusoidal wave profile and a constant water depth across the region of interest.

(b) Dispersion Relation: The dispersion relation encapsulates the interplay between the wave's frequency (or angular frequency) and its wavenumber. Within the linear theory, this relationship typically manifests as linear, signifying that waves of varying wavelengths exhibit disparate propagation speeds.

(c) Wave Velocity: Linear wave theory furnishes expressions for both the phase and group velocities of waves. The phase velocity denotes that at which individual wave crests propagate, while the group velocity delineates the rate at which the energy of a wave packet propagates.

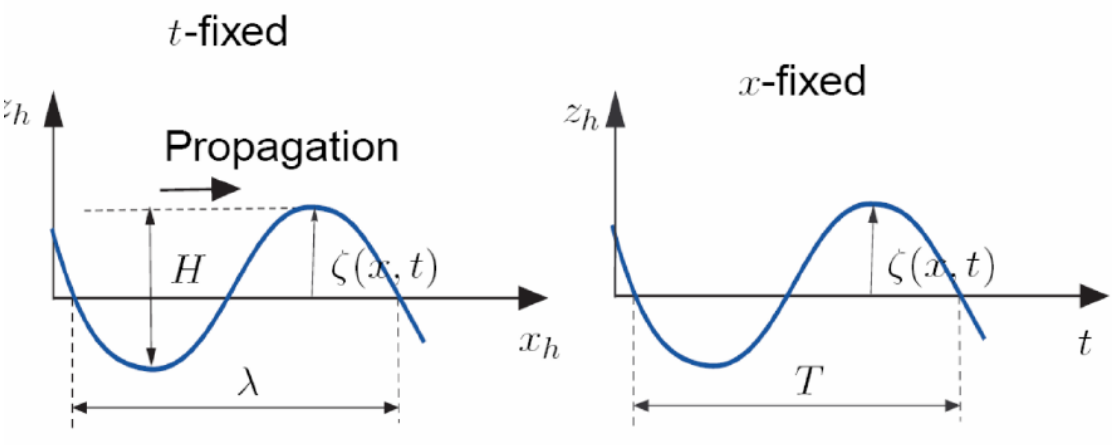

Figure 2.1 Wave Schematic diagram

$$\zeta(x,t) = asin(\kappa x - \omega t) \quad 2.1$$

ζ is the magnitude of the maximum displacement from the mean sea-level.

H is the wave height (m).

T is the wave period (s).

λ is the wavelength (m).

$a = \frac{H}{2}$ is the amplitude (m).

$\omega = \frac{2\pi}{T}$ is wave angular frequency (rad/s).

$k = \frac{2\pi}{\lambda}$ is wave number (rad/m).

$f = \frac{1}{T}$ is wave frequency (Hz).

$c = \frac{\omega}{k} = \frac{\lambda}{T}$ is wave crest/phase speed (m/s).

$\frac{H}{T}$ is the wave steepness.

Mass conservation with constant density hypothesis:

$$\nabla \cdot \vec{u}(x,z,t) = 0 \quad 2.2$$

Inviscid fluid:

$$\mu = 0 \quad 2.3$$

No viscosity means no vorticity. Therefore, the fluid is irrotational:

$$\nabla \times \vec{u} = 0 \tag{2.4}$$

If the velocity field is irrotational, it admits potential.

Hence, the velocity field can be written as the gradient of a potential function φ.

$$\vec{u} = \nabla\varphi \tag{2.5}$$

Then, the conservation of mass would become Laplace's equation:

$$\nabla^2\varphi = 0 \tag{2.6}$$

The Navier-Stokes momentum equation, under the hypothesis, can then be written and integrated into the space, becoming Bernoulli's equation:

$$\frac{\partial}{\partial t}\vec{u} + \vec{u}\cdot\nabla\vec{u} = -\frac{1}{\rho}\nabla p + \mu\nabla^2\vec{u} + \frac{1}{\rho}\vec{f} \tag{2.7}$$

$$\frac{\partial\varphi}{\partial t} + \frac{1}{2}(\nabla\varphi\cdot\nabla\varphi) + \frac{p}{\rho} + gz = C \tag{2.8}$$

And the boundary conditions:

(1) Dynamic boundary condition: Null pressure at the surface.

(2) Kinematic boundary condition: Particles on the surface remain there.

(3) Bed condition: No velocity component perpendicular to the sea bed.

Then the solution of the Air Theory

$$\eta(x,t) = a\cos k\,(x - ct) \tag{2.9}$$

$$\varphi(x,z,t) = \frac{ag}{kc\cosh(kh)}\cosh k\,(z+h)\sin k\,(x-ct) \tag{2.10}$$

$$c^2 = \frac{g}{k}\tanh(kh) \tag{2.11}$$

And Eq. 2.11 is the dispersion relation, which shows that harmonic waves with different wavenumbers and hence different wavelengths propagate at different speeds. And it can be written in another form:

$$\lambda = \frac{gT^2}{2\pi}\tanh\left(\frac{2\pi h}{\lambda}\right) \tag{2.12}$$

The definition of 'kh' leads to the definition of the ratio h/ λ (water depth/wavelength), which can be used to identify the water condition.

Table 2.1 Wave Parameter under Different Water Conditions

	Shallow Water	**Intermediate Water**	**Deep Water**
kh	$kh < 0.3$	$0.3 < kh < 3$	$3 < kh$
h/ λ	$h/\lambda < 1/20$	$1/20 < h/\lambda < 1/2$	$h/\lambda > 1/2$
Dispersion Relation	$\omega^2 = gk^2h$	$\omega^2 = gktanh(kh)$	$\omega^2 = gk$
λ vs T Relation	$\lambda = T\sqrt{gh}$	$\lambda = \frac{g}{2\pi}T^2 tanh(\frac{2\pi h}{\lambda})$	$\lambda = 1.56T^2$

In case of deep water: $C_g = \frac{C}{2}$

In case of shallow water: $C_g = C$

2.2 Point Absorber Mathematical Model

The original concept of the point absorber, introduced in 1975, describes a wave energy converter characterised by its compact size relative to the dominant wavelength in the ocean[21]. The initial definition did not detail the specific deployment setting, operational methodologies, or design features of such devices. Consequently, point absorbers exhibit versatility in their application, being adaptable for surface-level and submerged configurations, capable of employing singular or multiple structures for wave interaction, and functional across various operational modes.[22]

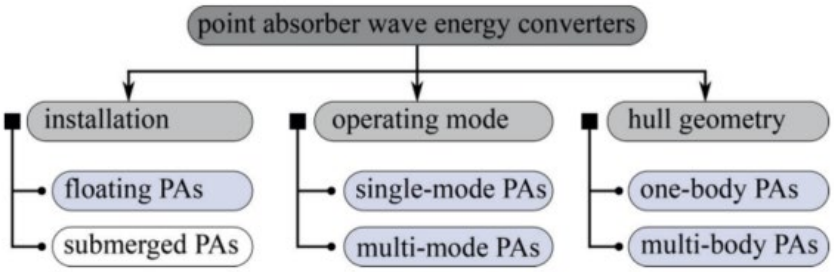

Figure 2.2 Point Absorber Classes

As said in Chapter 1, the point absorber framework stands out for its simplicity and potential, drawing significant attention from the global research community. This section is dedicated to presenting the mathematical modelling of point absorbers, focusing on hydrodynamic models.

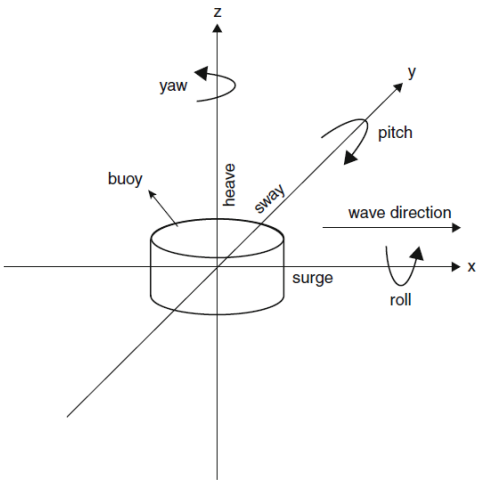

Figure 2.3 Schematic diagram of The Point Absorber Motion.

In unrestricted conditions, point absorbers can function across all six degrees of freedom: surge, sway, heave, pitch, roll, and yaw. However, some dominant oscillating modes exist for some point absorbers, which rely significantly on point

absorbers' geometric design. The point absorbers' geometry and dimensions significantly Influence their dynamics and performance, but this thesis work does not involve these aspects.

According to the linear wave theory, the fluid velocity potential can be divided into the incident, scattered, and radiated wave potential.

$$\phi = \phi_I + \phi_R + \phi_S \tag{2.13}$$

The force and force moment, on a structure in a fluid, is given by the fluid pressure integrated along the wetted surface S of the structure as follows:

$$F = \iint_S p dS \tag{2.14}$$

The total fluid pressure comprises the hydrodynamic pressure induced by the waves and the hydrostatic pressure. The hydrodynamic pressure can be written as:

$$p_{\text{dyn}} = -\rho\left(\frac{\partial \phi}{\partial t} + \frac{1}{2}(\nabla\phi)^2\right) \tag{2.15}$$

And in the linear potential flow theory, the non-linear term can be neglected. Then the equation becomes:

$$F_d = -\rho \iint_S \left(\frac{\partial \phi_l}{\partial t} + \frac{\partial \phi_S}{\partial t}\right) dS + \left(-\rho \iint_S \left(\frac{\partial \phi_R}{\partial t}\right) dS\right) \tag{2.16}$$

The first term represents the excitation force F_{e}, while the second term is the radiation force F_{r}.

The hydrostatic force F_s is caused by the fluid loading acting on a body when placed in still water.

$$F_s = -\rho \text{g} \iint_S z dS \tag{2.17}$$

From Newton's second law, the dynamic equation for an oscillating body may be written as

$$M\ddot{x} = F_e + F_r + F_s + F_{PTO} + F_c + F_m + F_v \tag{2.18}$$

M is the inertia of the oscillating body.

F_{PTO} denotes a PTO system, can be simplified as a linear spring-damper system, composed of PTO stiffness K_{PTO} and damping coefficients B_{PTO}.

$$F_{PTO} = -B_{PTO}\dot{x}(t) + K_{PTO}x(t) \qquad 2.19$$

F_c means a control force.

F_m represents the mooring force.

F_v is an unavoidable viscous effect.

If the mooring force is integrated into the PTO force and the viscous force to be neglected, it can be transferred into the frequency domain in the following form:

$$\left[-\omega^2\left(M + A_m(\omega)\right) - i\omega\left(B_{PTO} + B_{rad}(\omega)\right) + \rho g\pi R^2\right] = F_e \qquad 2.20$$

Where the added mass and radiation damping are given by the matrices$A_m(\omega)$ and $B_{rad}(\omega)$, respectively.

2.3 Technical Model

This section delves into the theoretical underpinnings and methodological approaches for analysing WEC arrays. Building on the foundations in preceding sections, where wave parameters were delineated through linear wave theory and the PA type WEC was modelled, the focus now shifts towards the comprehensive modelling of WEC farms.

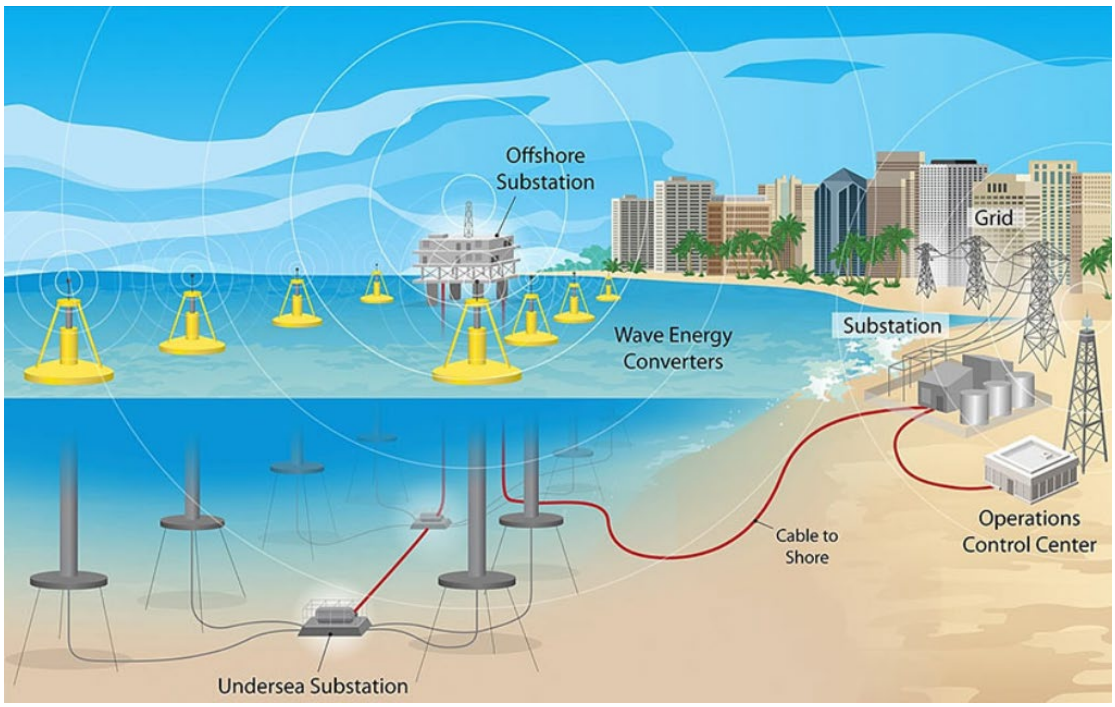

Figure 2.4 Artist's impression of a wave energy farm. Illustration by Alfred Hicks, NREL.

One of the advantages of WEC farms lies in their ability to consolidate essential infrastructures, such as power substations, mooring systems, and interconnecting cables. This collective utilisation of infrastructure streamlines the deployment process and yields substantial economies of scale, markedly diminishing initial capital outlays and ongoing operational costs.

Moreover, WEC arrays present an opportunity to exploit the hydrodynamic interactions among the devices, including wave diffraction and refraction phenomena inherent within the array configuration. When designed optimally, WEC farms can enhance the overall energy production through the strategic arrangement and orientation of the WEC units, allowing for the constructive interference of wave interactions and improving the power production from the waves.

2.3.1 Inter-array Interactions

As said, when WECs are placed in an incident wave field, they absorb energy and generate additional waves, such as diffracted and radiated waves. Notably, while the incident wave propagates as a plane wave in one direction, diffracted/radiated waves propagate in all directions from the source point. The energy conservation principle implies that the energy in these secondary waves comes from the incident wave. These secondary waves redistribute the energy initially moving in a single direction, altering the wave field around the WECs and affecting energy absorption.

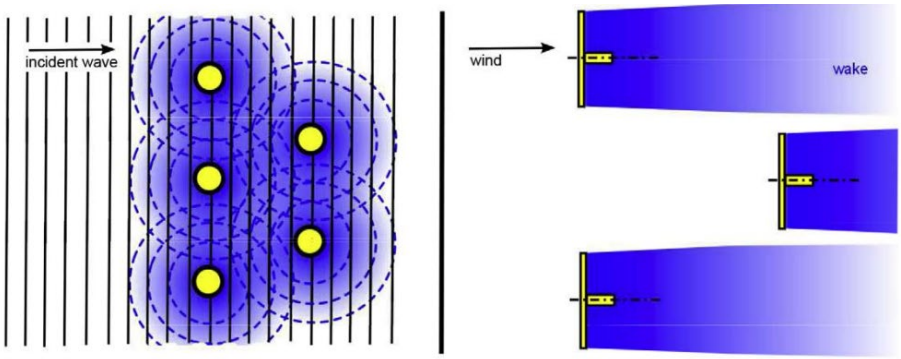

Figure 2.5 The interactions in the case of the WEC array and the wind turbine array

Regarding the wake effect, a critical difference between wind turbines and WECs is that in the latter, the disturbance of the wave field is observed not only behind the device but at every site around it. This indicates that all WECs in an array interact with each other regardless of their position. [23]

Therefore, the park effect in WEC arrays must be comprehensively considered due to the interconnected nature of wave interactions among the converters. Furthermore, the influence of these interactions diminishes with distance, suggesting that sufficiently spaced WEC units may operate with minimal interaction effects, and the wave energy flux eventually recovers to its calm state far from the WECs.

In recent years, more and more researchers have focused on this WEC farm effect, optimising the array configuration to improve the positive park effect. The most common methods for the WEC farm modelling can be divided into analytical, boundary elements, and physical experiments methods.

In 1977, Budal studied a buoy system, assuming that the floats were small enough to neglect interaction from scattered waves [24]. Later, in the 1980s, Evans introduced the

point-absorber approximation, which is still used today for wave energy array modelling due to its low computational costs. [25] [26]

In 1987, Mavrakos and Koumoutsakos used the iterative multiple scattering method for wave energy applications. [27] This method utilises isolated bodies' diffraction and radiation properties, adding iteratively reflected waves within an array until convergence. Combining this approach with the direct matrix method of Simon [28], Kagemoto and Yue [29] resulted in the direct matrix or multiple scattering method.

In 2015, McNatt coupled the analytical multiple-scattering method with a numerical method to accommodate arbitrary geometries. [30] Furthermore, advancements such as resonant modes [31] and interaction distance cut-offs have been introduced to enhance computational speed and optimise large arrays.

Due to advancements in computer performance, the Boundary Element Method (BEM) has become increasingly popular in recent years for modelling. In BEM, the boundaries of the fluid domain are discretised, and the integral representation of the fluid velocity potential is utilised. Boundary conditions on the body and free surface are applied, allowing the determination of fluid potential using Green's functions anywhere in the fluid domain. Many commercial software and open-source BEM packages have been developed to assist researchers in studying problems more efficiently and conveniently. [32] In 2010, Babarit [33] investigated WEC farm issues at Yeu Island in France using AQUADYN. Bozzi et al. [34] utilised AQWA to address the WEC farm problem in the Italian maritime area. Additionally, some BEM software has been integrated with wave propagation models such as MILDwave or OceanWave3D to analyse the perturbed wave field over a larger ocean area with varying bathymetry. [35]

Since analytical and numerical modelling inherently involve approximations and uncertainties, some researchers have conducted physical experiments to ensure an accurate understanding of systems and reliable results.

For instance, Thomas et al. [36] compared numerical predictions of the response of an array of five heaving floats in regular waves with experimental measurements. Weller et al. [37] conducted similar comparisons in irregular waves. Nader et al. [38] conducted experiments involving arrays of up to six point-absorber WECs, each moving in six

degrees of freedom, at the Australian Maritime College. In 2019, Bosma et al. [39] modelled two layouts of five fixed OWCs experimentally and numerically in regular and irregular waves. The layouts were selected based on previous layout optimisation studies, and the results showed a maximal power increase of 12%, referring to the non-optimal layout.

2.3.2 Point Absorber Approximation

Assuming that an array of N WEC devices constrained to undergo small oscillations in response to a long-crested incident wave train, with parameters including amplitude (A), radian frequency (ω), and angle of incidence (β), operates in water of infinite depth. Evans (1979) and Falnes (1980) demonstrated that the mean power absorbed per wave period by the array is contingent upon the wave train's incidence as

$$\boldsymbol{P}_{abs} = \frac{1}{8}\boldsymbol{X}^{*}\boldsymbol{B}^{-1}\boldsymbol{X} - \frac{1}{2}\left(\boldsymbol{U} - \frac{1}{2}\boldsymbol{B}^{-1}\boldsymbol{X}\right)^{*}\boldsymbol{B}\left(\boldsymbol{U} - \frac{1}{2}B^{-1}\boldsymbol{X}\right) \qquad 2.21$$

$\boldsymbol{X}$ is a column vector, denoting the complex time-independent component of the exciting force.

$\boldsymbol{U}$ is a column vector, denoting body velocity.

$\boldsymbol{B}$ is the radiation-damping matrix.

***** Denotes the complex conjugate transpose.

In this condition, $Re\{\boldsymbol{X}_m e^{-i\omega t}\}$ and$Re\{\boldsymbol{U}_m e^{-i\omega t}\}$ are exciting force on the mth body, due to the incident wavefield when all bodies are held fixed, and the velocity of the mth body respectively.

If the nondimensional displacement ratio vector is defined as $\boldsymbol{D}$, $Re\{\boldsymbol{A}\boldsymbol{D}_m e^{-i\omega t}\}$ is the displacement of the mth body. Then it can be used to represent the complex velocity $\boldsymbol{U}$ as:

$$\boldsymbol{U} = -i\boldsymbol{A}\omega\boldsymbol{D} \qquad 2.22$$

This means that the mean power extracted in Eq. 2.22 can be related to the displacements.

From the equation, we can also notice that the power absorbed would be maximised at the second term to be zero, which occurs when the velocity is:

$$\boldsymbol{U} = \frac{1}{2}\boldsymbol{B}^{-1}\boldsymbol{X} \qquad \mathbf{2.23}$$

In this condition, the power absorbed by the array would be:

$$\boldsymbol{P}_{opt} = \frac{1}{8}\boldsymbol{X}^{*}\boldsymbol{B}^{-1}\boldsymbol{X} \qquad \mathbf{2.24}$$

Then, we can introduce a q-factor, which is usually considered a key indicator of array performance and denotes the ratio of the performance of an array to that of N isolated devices, thus quantifying the effect of deploying the devices in an array.

When q < 1, the average power per WEC in the array is lower than that of an isolated WEC, indicating a destructive effect of wave interactions on power absorption within the wave farm. Conversely, when q > 1, the park effect becomes constructive.

$$q = \frac{\boldsymbol{P}_{abs}}{N\boldsymbol{P}_{opt,1}} \qquad 2.25$$

where $\boldsymbol{P}_{opt,1}$ is the optimal power absorbed by a single isolated device.

If we introduce another relative power measurement, absorption length:

$$\mathcal{L} = \frac{\boldsymbol{P}_{abs}}{\boldsymbol{P}_{w}} \qquad 2.26$$

where $\boldsymbol{P}_{w}$ is the mean power per unit crest width of the incident wave.

$$\mathcal{L}_{opt} = \frac{\boldsymbol{P}_{opt}}{\boldsymbol{P}_{w}} = \frac{\lambda}{2\pi}Nq \qquad 2.27$$

Then the q-factor can be written as:

$$q = \frac{2\pi}{\lambda N}\frac{\boldsymbol{P}_{opt}}{\boldsymbol{P}_{w}} \qquad 2.28$$

If considering an array with N devices, the q-factor equation at a specific angle of incidence β of this array can be represented by the exciting force:

$$q = \boldsymbol{X}_{\boldsymbol{m}}^{*}(\beta)\left[\frac{1}{2\pi}\int_{0}^{2\pi}\boldsymbol{X}_{\boldsymbol{i}}(\boldsymbol{\theta})\boldsymbol{X}_{\boldsymbol{j}}^{*}(\boldsymbol{\theta})\mathrm{d}\,\theta\right]_{mn}^{-1}\boldsymbol{X}_{\boldsymbol{n}}(\boldsymbol{\beta}) \qquad 2.29$$

where $*$ denotes complex conjugate, repeated subscripts denote summation and $[\,]_{mn}^{-1}$ denotes the (m, n)th term of the inverse of the matrix [ ]. A derivation of this result is given in Thomas and Evans.[40]

Considering exciting forces or far-field response determination is challenging, finding a simplifying approximation is appealing. In the point-absorber approximation, devices are considered small enough and widely spaced. In this case, the scattered waves are typically weak and tend to fade as they travel between devices, rendering them negligible.

The corresponding mathematical assumption is that ka << 1. Where k is the wave number, and a represents the radius of the WEC device. Previous research has demonstrated the validity of this approximation for ka $\leqslant$ 0.8, with a common value of ka = 0.4 adopted.[41] [42]Thus, the interaction problem of the WECs can be simplified, which allows the interaction factor to be expressed as

$$q = \frac{1}{N}\boldsymbol{\ell}^{*}\boldsymbol{\mathcal{J}}^{-1}\boldsymbol{\ell} \qquad 2.30$$

Where $\boldsymbol{\ell}$ is an N-component column vector with components:

$$\boldsymbol{\ell}_{\boldsymbol{m}} = e^{ikd_m\cos(\beta - a_m)} \qquad 2.31$$

$\boldsymbol{\mathcal{J}}$ is an N × N matrix with elements $\boldsymbol{\mathcal{J}}_{\boldsymbol{mn}}$ for devices operating in heave and generated by the zeroth order Bessel function of the first kind.

$$\boldsymbol{\mathcal{J}}_{\boldsymbol{mn}} = \boldsymbol{\mathcal{J}}_{\boldsymbol{0}}(\boldsymbol{k}d_{mn}) \qquad 2.32$$

In eq. 15 and 16, the variables m and n denote the specific device numbers out of N total devices. d_m is the distance from the origin point to the mth devices, $d_{mn}$is the distance between the mth and nth devices, a_m is the angle from the origin to the mth device.

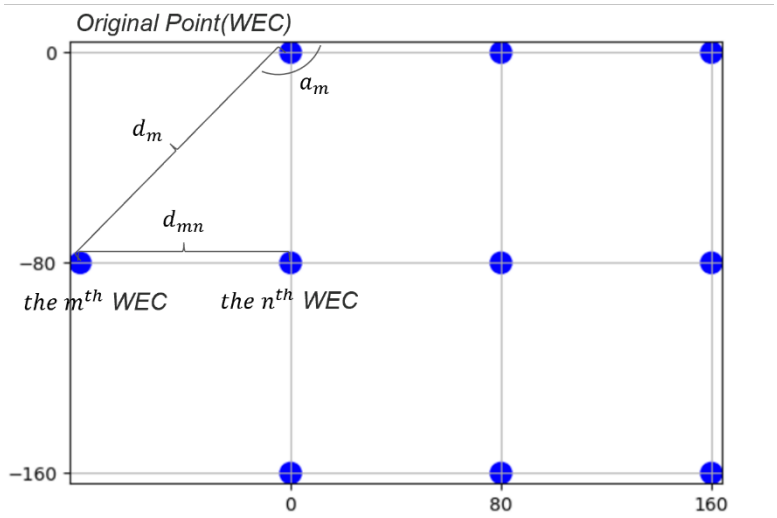

Figure 2.6 Schematic Diagram of A WEC Array

In this thesis work, the origin point is selected as the first device of the array. In this case, d_m is considered as the distance between the first and mth devices, and a_m is the angle between the first and mth devices.

With the point absorber approximation, the q-factor equation remains largely independent of body size.

However, given that a WEC farm project is a long-term project, in specific simulated array configurations where the q-factor > 1, the displacement of devices within the array may reach incredibly large values during some time slices. While these larger displacements may capture more wave energy, they also pose risks under certain conditions.

Therefore, it may be necessary to limit body displacements to ensure they do not exceed a specified multiple of the incident wave amplitude. We have introduced the nondimensional displacement ratio vector $\boldsymbol{D}$ before, and here Thomas and Evans [40] propose the equation of it at optimal tuning:

$$\boldsymbol{D} = -\frac{i}{2\omega A}\boldsymbol{B}^{-1}\boldsymbol{X} \qquad \mathbf{2.33}$$

The exciting force on a device due to an incident wave propagating in the direction θ = β may be related to the far-field behaviour of the corresponding radiation potential through the Haskind relationship. [43]

$$\boldsymbol{X_m} = -\frac{4\rho g A c_g}{k}\boldsymbol{f_m}(\beta + \pi) \quad 2.34$$

$$\boldsymbol{B_{mn}} = \frac{k}{16\pi P_w}\int_0^{2\pi}\overline{\boldsymbol{X_m(\theta)}}\,\boldsymbol{X_n(\theta)}d\theta \quad 2.35$$

where g is the acceleration due to gravity, c_g is the group velocity, and $\boldsymbol{f_m}$ is an angular function. Following the point absorber approximation the scattering of the radiated waves within the array is neglected so that the far-field of the waves radiated by a particular device is unaffected by the presence of the remaining devices. This implies that if $\boldsymbol{f_m}$ is known for one body, it holds for all other bodies in the array, particularly when considering arrays of identical bodies operating in the same mode. [43]

$$\boldsymbol{f_m(\theta)} = \boldsymbol{f(\theta)}e^{-ikd_m cos\,(\theta - a_m)} \quad 2.36$$

$\boldsymbol{f(\theta)}$ is known analytically for a single heaving semi-immersed sphere. The solution has been given by Havelock in 1955.

$$\boldsymbol{f(\theta)} = ka^2(2\pi)^{\frac{1}{2}}\Omega e^{-\frac{1}{4}i\pi + ix} \quad 2.37$$

Where k is the wave number, and a is the radius of the device. As we can see that $\boldsymbol{f(\theta)}$ is independent of $\boldsymbol{\theta}$.

$$\Omega e^{-\frac{1}{4}i\pi + ix} = \Omega e^{ix} \times e^{-\frac{1}{4}i\pi} \quad 2.38$$

It is depended on ka; Havelock had used constant C and D to define it at the condition ka = 0.4.

$$\Omega e^{ix} = C - iD \quad 2.39$$

$$C = 0.3029, D = -0.0486\ ^{44} \quad 2.40$$

Finally, we back to eq.17, the nondimensional displacement ratio vector $\boldsymbol{D}$ could be calculated.

2.4 Economic Model

The European Strategic Energy Technology Plan declaration of intent for ocean energy includes ambitious economic targets for wave and tidal energy technologies. Specifically, wave energy technologies are expected to achieve an LCoE of 200 EUR/MWh by 2025, 150 EUR/MWh by 2030, and 100 EUR/MWh by 2035. [45] These targets represent ambitious goals, indicating significant potential for economic improvement in wave energy.

Technology Readiness Level (TRL) and Technology Performance Level (TPL) are widely used to evaluate new technologies' maturity level and techno-economic performance. These frameworks aid in assessing progress from conceptual stages to mature fully and operational states, facilitating decision-making for further development, investment, and deployment. According to a report by the US National Renewable Energy Laboratory in 2021, the TPL level of the point absorber model falls between 4 and 5, indicating a moderate level. To achieve economic viability under various market and operational conditions, several key technology implementations and fundamental conceptual improvements are necessary and considered feasible. [46] In the EU, The LiftWEC project has developed an LCoE calculation tool for WEC farms to assist projects in the early stages of TRL development in conducting economic evaluations. [47]

Moreover, considering the constructive park effect mentioned in the previous section, many researchers have proposed using Economical Objective Functions to optimise WEC geometry, array layout, and control strategies. Piscopo et al. [48] conducted LCoE optimisation focusing on point absorber dimensions. Giassi et al. [49]. proposed a detailed economic model that considers various factors such as power output, device dimensions, number of WECs, array layout, water depth, distance to shore, electrical configurations, offshore work, and cabling. Guanche et al. [50]. estimated operation and maintenance costs in relation to the placement of wave energy parks.

In this thesis work, an economic model has also been developed to optimise array layout and evaluate results based on CAPEX, OPEX, and LCoE.

2.4.1 Cost function

CAPEX often refers to the initial investment needed to acquire physical assets for a project and external non-technological costs—all the spending related to project development, deployment, and commissioning before the operation.

The sub-costs of the CAPEX in this work involve (a) Devices, (b) PTO, (c) Foundations and Moorings, (d) Grid connection, and (e) Installation and Decommissioning.

Table 2.2 Cost Function and Parameters

C	Category	Cost Function (Unit)	Source
C_D	WEC Device	1,540,000 (EUR/MW)	[51]
C_{PTO}	PTO	Hydraulic: 800 (EUR/MW)	[52]
		Linear generator: 600 (EUR/MW)	
		Mechanical: 1,400 (EUR/MW)	
		Air turbine: 1,000 (EUR/MW)	
C_F	Foundations	0 < Depth < 30: $0.15 + 10^{-5}d^3$ (MEUR/MW)	[47]
		30 < Depth < 60: $0.35 + 4\times10^{-5}d^3$ (MEUR/MW)	
		60 < Depth: $0.15 + 0.016d$ (MEUR/MW)	
C_M	Moorings (CALM)	$0.265\times9.81Ld^2K$	[53]
$C_{G,MVAC}$	In-Array Cable	$L_{MVAC} \times (a_1 V_{MAC} + b_1)$	[54]
$C_{G,HVAC}$	Export Cable	$1.452 \times (AP_{Cab}^2 + BP_{Cab} + C + D)$	[55]
C_{Ins}	Installation Cost	WEC: 10,000 (EUR/MW)	[51]
		MV Cable: 380 (EUR/Meter)	[54]
		HV Cable: 750 (EUR/Meter)	
		Offshore Substation: /	
C_{Dec}	Decommission Cost	$88\% \times C_{Ins}$	[56]

(1) For C_M. the L in the cost function is the length in meters, d is the diameter in mm, and K is a factor.
(2) For $C_{G,MVAC}$, the a1 and b1 in the cost function are factors.
(3) For C_{Ins}, the A, B, and C are factors.

In case of using mooring line for WEC farm:

$$CAPEX = C_D + C_{PTO} + C_M + C_{G,MVAC} + C_{G,HVAC} + C_{Ins} + C_{Dec} \quad 25$$

In case of using Functions structure for WEC farm:

$$\text{CAPEX} = C_D + C_{PTO} + C_F + C_{G,MVAC} + C_{G,HVAC} + C_{Ins} + C_{Dec} \quad 26$$

OPEX encompasses ongoing costs incurred during the regular operation of a project or business. It includes expenses such as labour salaries, utilities, maintenance, supplies, and other day-to-day operational expenses necessary to sustain the functioning of the project or business.

In this work, OPEX is calculated based on CAPEX through an OPEX factor. This factor is roughly divided into four levels based on the technology's maturity and the project's scale.

Table 2.3 OPEX Factor Table

State	OPEX Factor	**Source**
Single Device	8 %	[57] [58]
Small Array	6 %	
Utility Scale	4.5 %	
High Maturity	1.44 %	

$$\text{OPEX} = OPEX\ Factor \times CAPEX \quad 2.41$$

2.4.2 Levelized Cost of Energy

It is a crucial metric to evaluate the economics of generating electricity from a particular project. It represents the per-unit cost of electricity over the project's entire lifetime, including all CAPEX, OPEX and other relevant expenses.

This metric effectively highlights variations in electricity costs across different energy technologies, revealing gaps between wave energy and other renewable energies. It assists policymakers and investors in making informed decisions regarding energy

investments based on economic viability and, additionally, guides researchers in identifying the correct direction for improving wave energy technology.

In general terms, the LCOE is defined as

$$LCOE = \frac{CAPEX + \sum_{t=1}^{n} \frac{OPEX_t}{(1+r)^t}}{\sum_{t=1}^{n} \frac{AEP_t}{(1+r)^t}} \quad 2.42$$

Where r is the discount ratio, t is the project lifetime, and AEP is the annual energy production.

Chapter 3: Site Selection

3.1 Metocean Conditions

Waves on the ocean are primarily generated by the wind. When wind blows across the water's surface, it transfers some of its energy to the water, creating tiny ripples. These ripples, if the wind persists, gradually evolve into waves. However, waves reach a point where their growth plateaus due to energy losses, like white capping, which balances the wind’s energy input. The size and strength of waves depend on factors such as wind speed, duration, fetch (the distance over which the wind blows), and the ocean floor's depth and contour. Tides, currents, and seismic activity also play roles in wave formation, making ocean waves a complex interplay of forces.

Natural oceanic waves are unpredictable and diverse, making it challenging to accurately harness and quantify their energy. To address this, researchers develop wave models that simulate different ocean wave behaviour. These models enable researchers to generate long-term data on wave climates, which is essential for deploying WECs and other offshore engineering projects, while deploying natural wave measurement instruments to produce long-term data is often complicated and costly.

The initial quantification of wave generation began with the relationships established by Sverdrup and Munk, which correlated wind speed, fetch, time, wave height, and period.[59] Bretschneider later refined this approach, leading to the development of the widely used SMB method.

In 1952, a significant breakthrough occurred when Pierson and Marks proposed describing sea conditions as the superposition of sinusoidal waves, each defined by frequency, direction, and height. This concept provided a more comprehensive understanding of wave behaviour in a given area and at a given time.

Building upon these advancements, complementary theories on wave generation emerged by Phillips and Miles. Hasselmann [60] furthered this research by quantifying the interactions and conservative exchange of energy among spectral components.

Subsequently, an empirical expression for white-capping energy loss was proposed based on the formulation of the input function and the JONSWAP experiments. [61]

With the development of the reduced Discrete Interaction Approximation parameterisation for non-linear interactions [62] and the development of third-generation systems like the Wave Model, wave modelling is seen as moving towards maturity. [63]

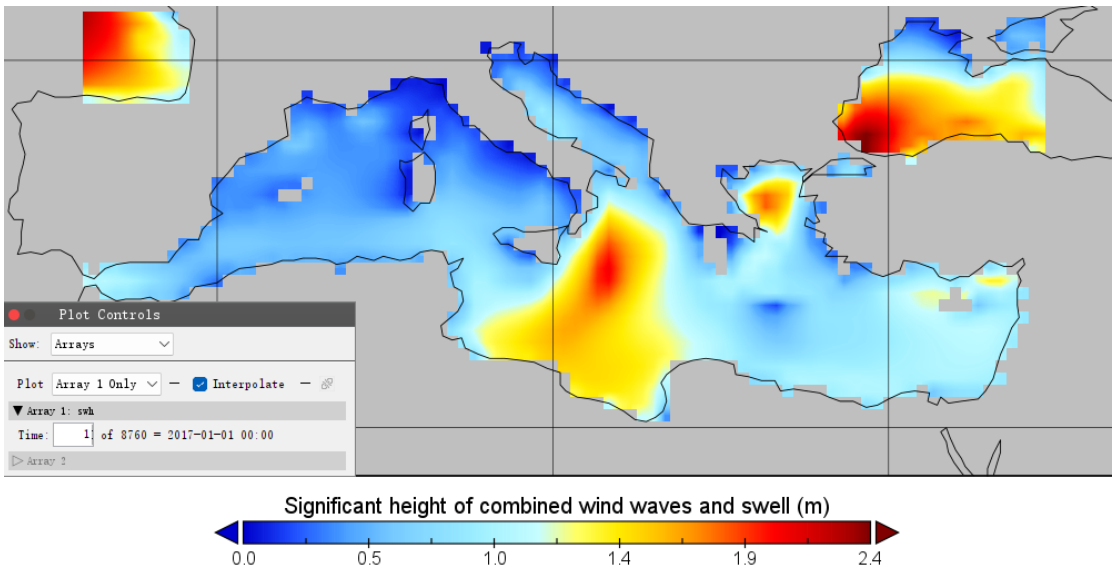

Figure 3.1 Contour Plot of Significant Wave Height at 2017.01.01 From the Dataset

The following is information on databases or wave models used in the references.

Table 3.1 Databases Used in the References

Dataset	**Spatial Resolution**	**Interested Area**	**File Type**	**Referenc**
IHCantabria-GOW2	0.25° × 0.25°	Global	NetCDF	[64]
WAVERYS	0.2° × 0.2°	Spain and Portuguese Coast	NetCDF	[65]
POSEIDON System		North Aegean Sea	NetCDF	[66]
ERA-Interim	0.75° × 0.75°	UK Atlantic and North Sea	NetCDF	[67]
MARENDATA Platform	0.5° × 0.5°	West Coast of Africa	NetCDF	[68]
WaveWatch III		South-east Australian coast	NetCDF	[69]

For this thesis work, ERA5 is employed, which is the latest available ECMWF reanalysis dataset and provides comprehensive data for various macro-areas, including waves, wind, and solar parameters. This dataset spans from 1979 to the

present, typically offering a temporal resolution of 1 hour. However, it maintains a relatively low spatial resolution, approximately 50 km. The time parameter utilised in this work corresponds to that available in the MORE-EST Platform, maintaining an hourly temporal resolution from 2010 to 2019. [70]

3.2 Site Selection Methods

As mentioned, WEC is a device that harnesses kinetic energy from waves and converts it into energy. However, the distribution of wave energy resources is uneven globally due to the ocean's vastness, covering approximately 70% of the Earth's surface. Defining suitable sites for deploying WEC farms is a critical challenge.

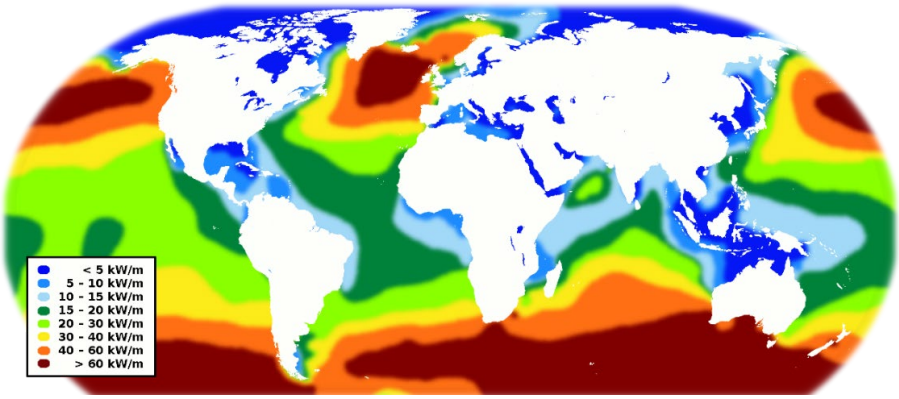

Figure 3.2 World Wave Energy Resource Map

Roughly, site selection methods can be categorised into three types. The first method is Direct Selection, where sites are chosen based on the mean wave power density [Pw] derived from wave parameters such as significant wave height [Hs] and wave period [Te]. This method is commonly employed in early-stage research. [71] [72]

The second method evaluates sites based on one or more indexes, which can be obtained through nonlinear mathematical operations on wave parameters or via statistical methods. For instance, Kumar et al. [73] utilised a variation index (MVI/SVI/AVI) to assess the spatial-temporal variation of wave energy resources in the Indian Ocean region. Lavidas, G., [74] on the other hand, introduced a statistical factor called 'SIWED', derived from wave parameters, to evaluate the variability, survivability, and energy production potential of local wave energy resources.

The third approach is the Multi-Criteria Approach. Similarly, the site can be evaluated by indexes that are generated by statistical methods. However, something different from the previous method is that these indices relate not only to the wave parameters but also to encompass various aspects such as structural survivability, installation and maintenance accessibility, distance to the shore, and others. Finally, these diverse criteria are combined through weighted aggregation to obtain the final assessment result. [75]

Alternatively, criteria such as wave energy resources, water depth, seabed characteristics, distance to the shore, and vessel density can be directly divided into intervals by setting thresholds, each corresponding to different levels and scores. [69] Expert opinions or empirical rules are then used to weigh the scores of all criteria and rank them to select the most suitable deployment sites. However, the subjective nature of the weighting process may compromise the fairness and accuracy of decision-making. Considering this, currently, some researchers propose using probabilistic models such as Bayesian networks [76] or Monte Carlo [67] methods to replace previous empirical rules or expert opinions.

Here, we adopted a Semi-Multi-Criteria Approach for the thesis work and developed a QGIS and Python selection tool. Specifically, various criteria, including wave parameters, accessibility, monthly variation index, water depth, seabed characteristics, distance to the shore, and vessel density, are directly divided into intervals by thresholds without scoring or weighting, which reduces subjectivity in the selection process decouples the assessment parameters, simplifying the selecting process, comparing with the whole Multi-Criteria Approach.

Subsequently, QGIS is utilised to perform the final site assessment. Benefiting from the interactivity of QGIS, users can adjust the interval thresholds to meet specific assessment requirements for different sea conditions. Additionally, restrictive selection criteria related to ecological conservation regulations, industrial needs, or military requirements are also incorporated into this tool.

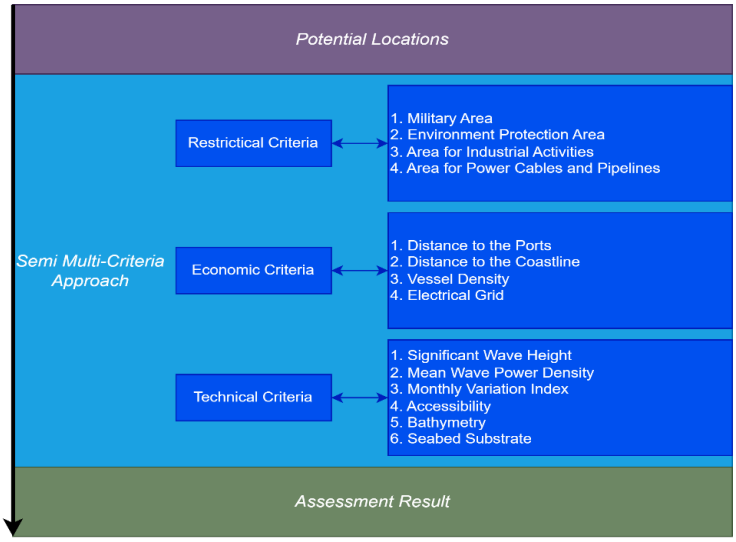

Figure 3.3 Site Selection Process in This Work

3.3 Datasets/Databases and Selection Criteria

In accordance with the former sections detailing the site selection method and process, this section will proceed with introducing datasets and databases used in sub-section 1. Subsequently, sub-section 2 will present the thresholds set for each criterion.

3.3.1 Datasets and Databases

In this thesis work, the datasets and databases are classified into two kinds: (a) Origin Data or Non-Processable Data and (b) Processable Data.

(a) The Origin Data or Non-Processable Data refers to the wave data sourced from ECMWF - ERA5 as introduced in Section 3.1 and the datasets utilised to construct the base map. These include the world map, coastline, and exclusive economic zone datasets. These data are fixed and cannot be adjusted by the users.

Table 3.2 Wave Databases and Datasets for The Base Map

Data	**Datasets and Databases**	**File Type**	**References**
Wave Data	ECMWF - ERA5	NetCDF	[70]
World Map	Natural Earth	TIFF	[77]
Coastline	Natural Earth	Shapefile	[77]
Exclusive Economic Zone	Marine Regions	Shapefile	[78]

Figure 3.4 The Base Map

(b) The processable data are used to establish the criteria for site selection. In detail, related raw datasets are obtained from organisations for criteria like bathymetry,

vessel density, etc., which would be further reprocessed by Python, involving tasks such as setting interval thresholds, filtering out non-compliant data, and generating new raster or vector files for input into QGIS for site assessment.

Based on the kinds of selection criteria, these can be categorised into three types: 1. Restrictive Sector Data, 2. Economic Sector Data, and 3. Technical Sector Data.

Table 3.3 Datasets for Selection Criteria

Category	**Data**	**Datasets and Databases**	**File Type**	**Refer**
Restrictive Sector Data	Power Cables	EMODnet Human Activities	Shapefile	[79]
	Power Cables Buffer Area	Reprocessed data	Shapefile	/
	Pipelines	EMODnet Human Activities	Shapefile	[80]
	Pipelines Buffer Area	Reprocessed data	Shapefile	/
	Military Area	EMODnet Human Activities	Shapefile	[81]
	Environment Protection Area	EMODnet Human Activities	Shapefile	[82]
	Area for Oil and Gas exploitation and exploration	EMODnet Human Activities	Shapefile	[83]
	Area for Oil and Gas exploitation and exploration Buffer Area	Reprocessed data	Shapefile	/
Economic Sector Data	Port Points	EMODnet Human Activities	Shapefile	[84]
	Distance to the Coastline	Reprocessed data	Shapefile	/
	Vessel Density @ 2022	EMODnet Human Activities	TIFF	[85]
	Electrical Grid	Interconnected network of Continental Europe	PDF	[86]
Technical Sector Data	Significant Wave Height	ECMWF - ERA5	NetCDF	[70]
	Mean Wave Power	ECMWF - ERA5	NetCDF	[70]
	MVI @2020	Reprocessed data	NetCDF	/
	Accessibility @2010 to 2020	Reprocessed data	NetCDF	/
	Bathymetry	GEBCO	NetCDF	[87]
	Seabed Substrate	EMODnet Seabed Substrates	Shapefile	[88]

From the table above, it is evident that apart from the datasets reprocessed by Python, most datasets are from two platforms: Natural Earth and EMODnet. Natural Earth is an open-source database platform housing a rich collection of geographic information data. EMODnet (European Marine Observation and Data Network) operates as an open-source network comprising organisations collaborating to enhance Europe's marine data infrastructure. This network encompasses diverse marine datasets, including Bathymetry, Biology, Chemistry, Geology, Human Activities, Physics, and Seabed Habitats.

3.3.2 Selection Criteria

This sub-section will discuss the reprocessing action for the raw datasets in Python. The thresholds for each criterion will be introduced to filter out non-compliant data and set intervals to identify the data quality.

Many studies utilising the Multi-Criteria Approach for site selection have provided some information for thresholds setting. For instance, Maldonado et al. [65] pointed out some thresholds for specific criteria for the site assessment of the ocean near Spain and Portugal. The restrictive threshold for distance to the shore was set at less than or equal to 600 km, with interval thresholds at 30 km, 100 km, and 600 km, normalising a criterion at a specific site. Regarding bathymetry, the restrictive threshold ranged from -100 to -60 m, with Seabed Geology categorised into five levels based on characteristic features.

Weiss et al. [64] and Lavidas [74] defined thresholds related to wave energy resources. The restrictive threshold for significant wave height was 1 to 6 meters and 0.5 to 4 meters, respectively. The restrictive threshold for wave power density was established as more important than or equal to 15 kW/m. Additionally, Lavidas has defined the restrictive threshold for Accessibility for installation and maintenance based on significant wave height, ensuring that at least 70% of the time, significant wave height is within 0 to 1.5 meters.

The restrictive and interval thresholds and corresponding actions in this thesis work are listed below.

Table 3.4 Restrictive and Interval thresholds for Selection Criteria

Category	**Criteria**	**Restrictive Threshold**	**Interval Threshold**	**Action**	**References**
Restrictive Sector Data	Power Cables Buffer Area	Buffer @ 500 m	/	Exclusion	[65][89][90]
	Pipelines Buffer Area	Buffer @ 500 m	/	Exclusion	[65][89]
	Military Area	/	/	Exclusion	[90][91]
	Environment Protection Area	/	/	Exclusion	[65][89][90][91]
	Area for Oil and Gas exploitation and exploration Buffer Area	Buffer @ 500 m	/	Exclusion	[65][90]
Economic Sector Data	Distance to the Port	/	/	Evaluation	/
	Distance to the Coastline	/	50 km, 100 km, 150 km, 200 km	Evaluation	[90][92]
	Vessel Density @ 2022	The busiest 0.5% area		Exclusion	[89]
	Electrical Grid	/	/	Evaluation	/
Technical Sector Data	Significant Wave Height	Suitable Range: ⌈0.5, 4⌉ m	/	Exclusion	[74][93]
	Mean Wave Power	Suitable Range: ⌈5, +∞) kW/m	/	Exclusion	[90][92]
	MVI @2020	The most unstable 40% area	/	Exclusion	[94]
	Accessibility @2010 to 2020	Suitable Range: ⌈60%, 100%⌉	/	Exclusion	[74]
	Bathymetry	Suitable Range: ⌈-300, 0⌉ m	/	Exclusion	[89]
	Seabed Substrate	/	/	Evaluation	[65][89]

(1) The “Exclusion” action means that if one data of a site is over the corresponding threshold(s), this site should be filtered out.
(2) The “Evaluation” actions mean that several intervals would be generated based on the thresholds set, and each interval represents a quality level.

3.4 Results in QGIS

With the availability of datasets, databases, and set thresholds, the reprocessing task can be conducted using Python. Subsequently, the newly generated vector and raster files would be inputted into QGIS for visualisation.

(a) Restrictive Sector Selection

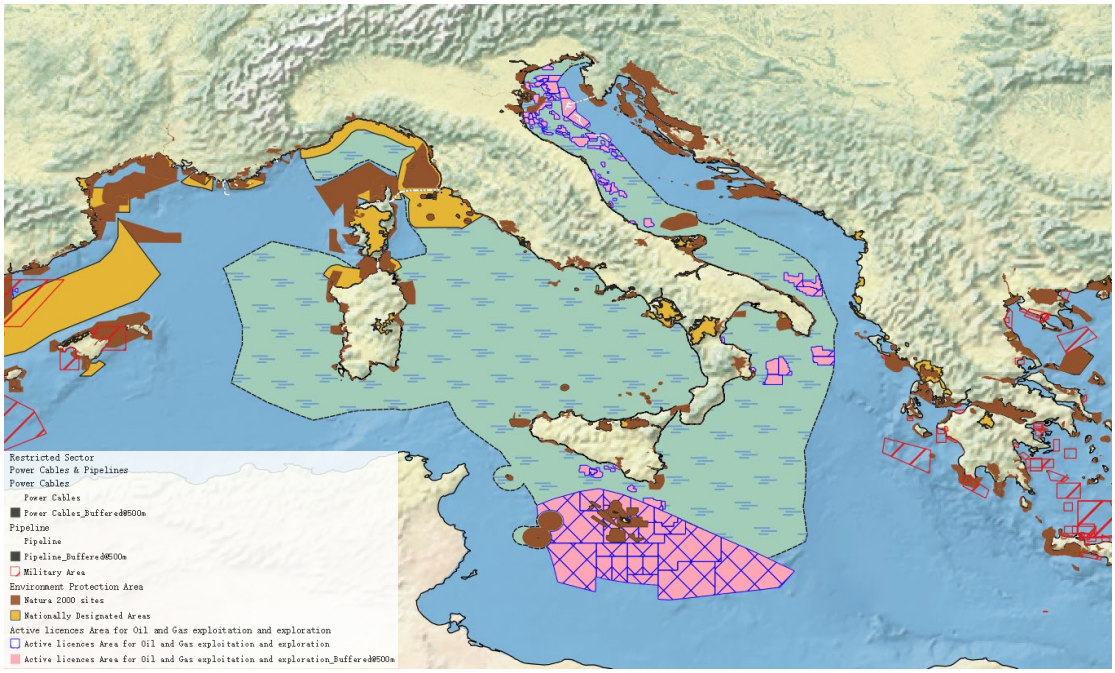

Figure 3.5 Restrictive Sector Selection In QGIS

Identifying and considering restricted areas are vital in the site selection process for WEC farm deployment, as specific sites are strictly prohibited, regardless of their suitability. These restricted areas are off-limits due to various factors such as environmental conservation, military safety regulations, or existing industrial infrastructure. Ensuring compliance with these restrictions is essential to prevent potential conflicts, minimise environmental impacts, and adhere to legal requirements while deploying WEC farms.

In this work, the restrictive sector also considered the buffer area around existing industrial infrastructures (Pipelines, Power Cables, and Oil and Gas exploitation and exploration Area) based on References [65] [89] [90] to ensure the relative safety of the existing facilities and to provide space for their future development while meeting planning policies. The buffer area range was set at 500 meters and implemented in Python using the "Buffer function". *(Code Segment Example is shown in Appendix)*

(b) Economic Sector Selection

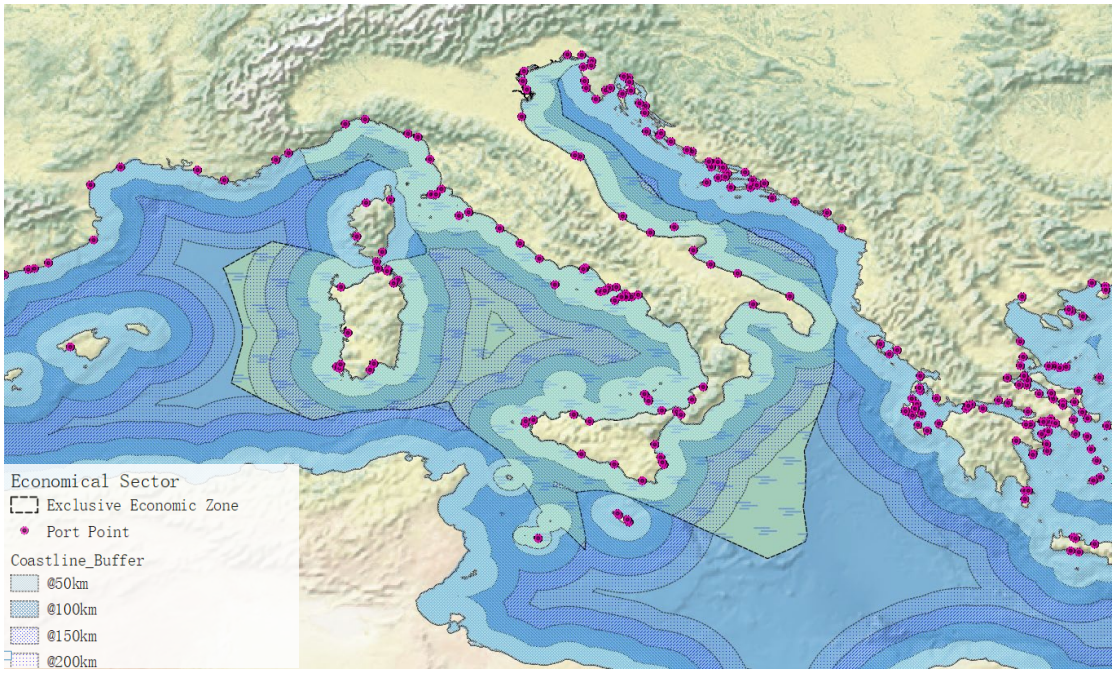

Figure 3.6 Economic Sector Selection: Distance to Shore and Ports in QGIS

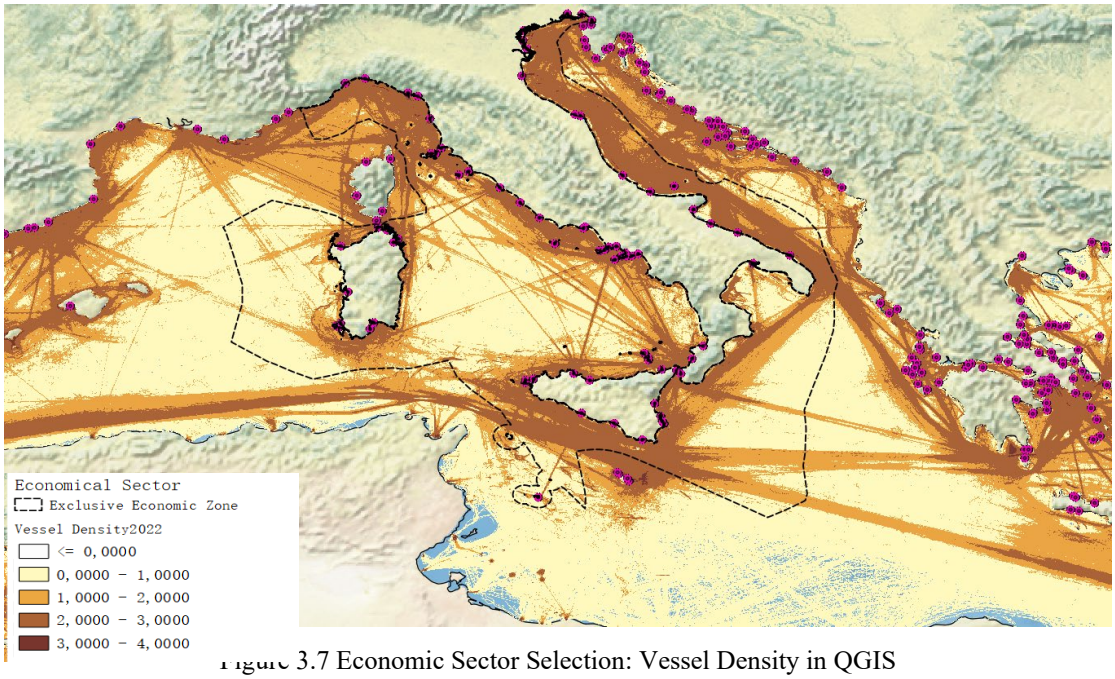

Figure 3.7 Economic Sector Selection: Vessel Density in QGIS

The economic sector plays a role in influencing the expenses associated with installing and maintaining WEC farms. These criteria include the distance to the coastline, proximity to ports, access to the local power grid, and vessel density, which are included in this thesis work.

The distance to the coastline, ports, and power grid-primarily impacts economic aspects, while vessel density is related to safety concerns for both WEC devices and

ships. Typically, operational and maintenance expenses for WEC farms increase with greater distance from the coastline. Conversely, sites closer to ports offer lower costs and greater convenience for construction and setup, making them more favourable for establishing WEC farms. Additionally, the distance from the local power grid affects expenses related to connection fees and can also influence power conversion efficiency.

The distance to the coastline is realised by establishing a buffer area for the shoreline in Python. While the vessel density is quantified and evaluated by setting several intervals. *(Code Segment Example is shown in Appendix)*

(c) Technical Sector Selection

The technical criteria focusing on the power density for offshore wave energy site selection are widely acknowledged standards, and they can provide a simple and intuitive indication of the potential of local wave energy resources. In this work, besides the criteria of wave power density and significant wave height, four additional criteria are introduced: Monthly Variation Index, Installation and Maintenance Accessibility, Bathymetry, and Seabed Substrate.

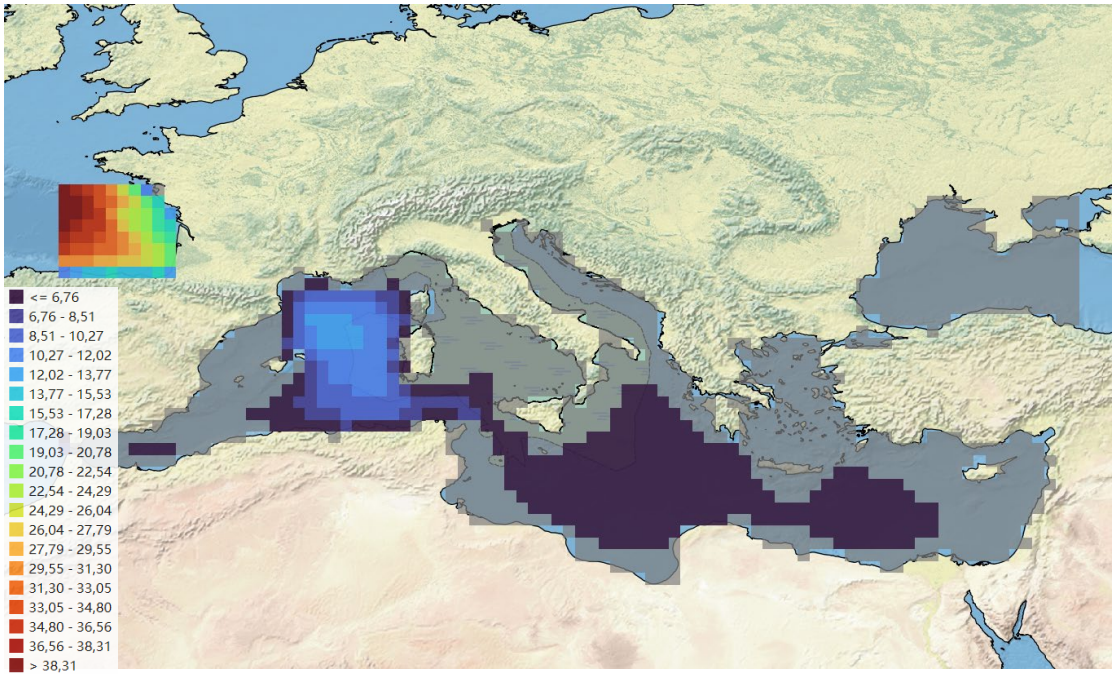

Figure 3.8 Technical Sector Selection: Mean Wave Power Density In QGIS

The Monthly Variation Index represents the variability of wave energy resources, and the equation is derived from Reference [80]. It assists in quantifying the variability of wave energy resources, offering valuable insights into their temporal fluctuations.

$$MVI_j = \frac{(P_{max} - P_{\min})_j}{P_{aj}} \quad 3.1$$

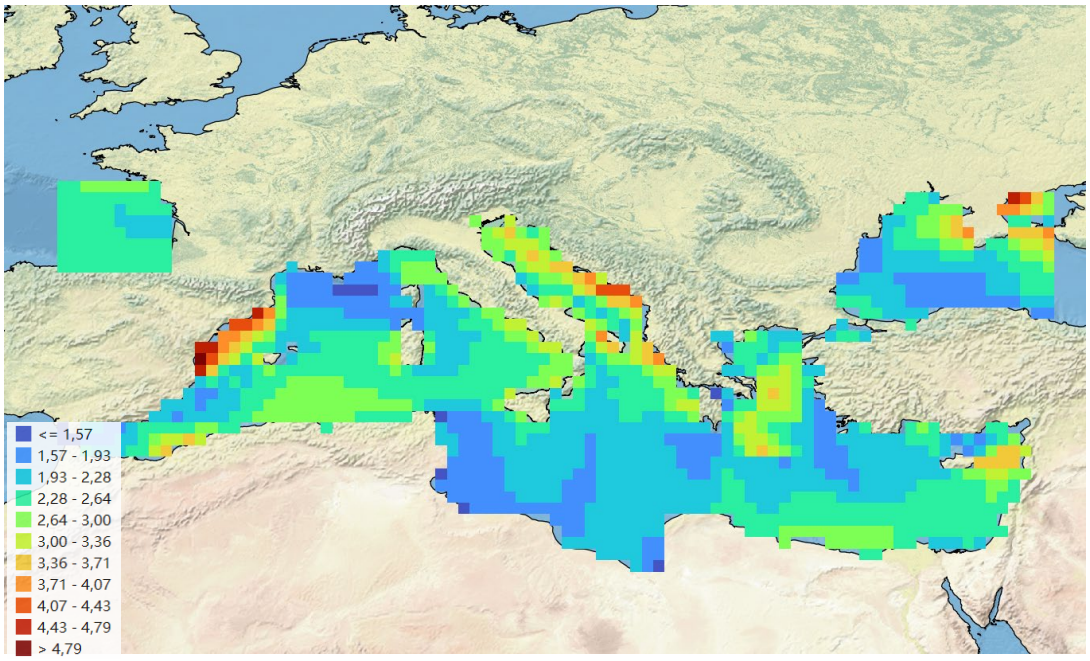

Figure 3.9 Technical Sector Selection: Monthly Variation Index In QGIS

Accessibility denotes the ease of installation and maintenance operations at a given site. Unlike onshore projects, ocean weather conditions significantly influence offshore projects, and adverse wave environments may directly lead to increased devices and labour costs. In this work, the threshold for accessibility is set at 60%, meaning that if a site is accessible 60% of the time, it is considered acceptable.

The introduction of the Bathymetry criterion considers the current technical limitations of WEC devices. In sites with greater water depths, complex wave conditions may affect the normal operation of WEC devices and increase installation costs.

Lastly, the seabed substrate represents the underwater environment of the local marine area. Considering that WEC devices must use mooring systems or foundations, seabed substrate directly affects the suitability and feasibility of device deployment and operation. The composition and stability of the seabed substrate affect the anchoring and stability of WEC devices, as well as the efficiency and effectiveness of

normal operation. Additionally, seabed substrate characteristics such as sediment type, topography, and geological features impact the installation process, maintenance requirements, and long-term performance of WEC systems.

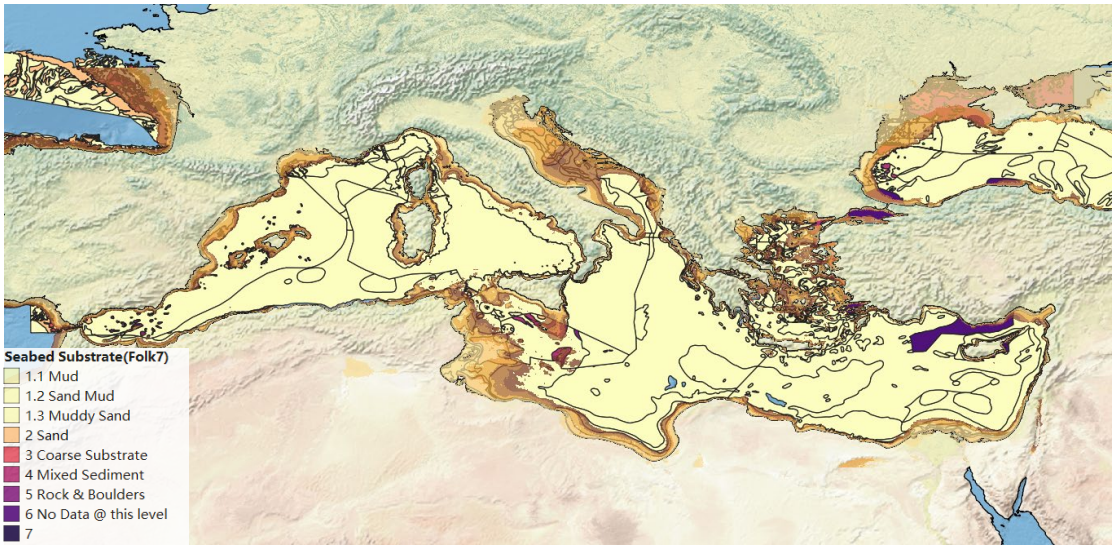

Figure 3.10 Technical Sector Selection: Seabed Substrate In QGIS

We can visualise the final site assessment map in QGIS with all selection criteria introduced. As shown in the image below, the sites, circled in red, represent the sites within the exclusive economic zone of Italy that satisfy all technical criteria. The colour bar is based on wave power density in kW/m. This visualisation was achieved by overlaying a mask over all sites that did not meet the specified thresholds using the "Mask function" in Python. *(Code Segment Example is shown in Appendix)*

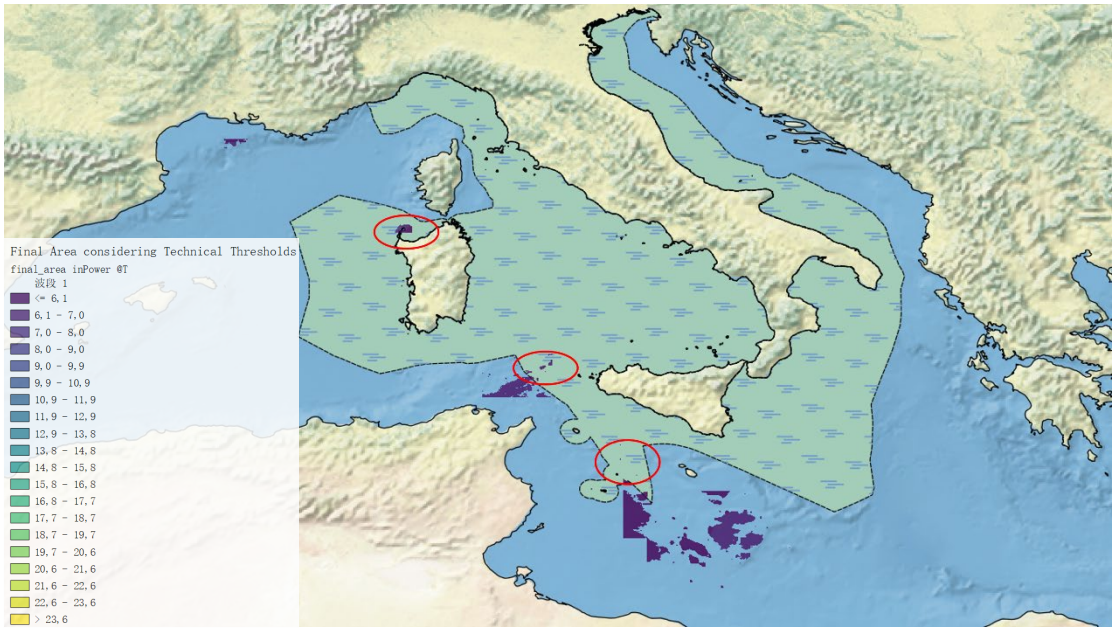

Figure 3.11 Final Site Assessment Map in Wave Power Density In QGIS

The figure shows that these three areas are located north of Sardinia Island, west of Sicily Island, and south. Then, we consider the Restrictive Sector criteria by overlaying the Restrictive Sector layer onto the former map to finalise the site selection process. This step allows to ensure that the final selected sites do not overlap with any restricted areas, thus complying with relevant regulations and minimising potential conflicts.

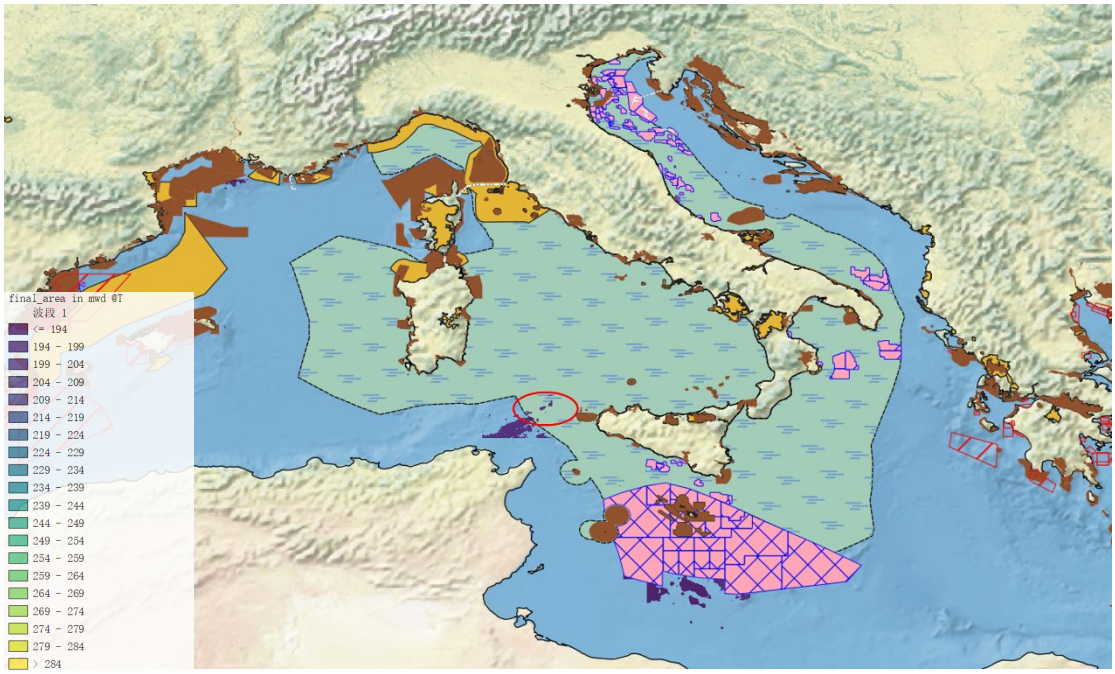

Figure 3.12 Final Site Assessment Map in Mean Wave Direction with Restrictive Sector Criteria Consideration In QGIS

As depicted in the above figure, the colour bar on this site selection map can also be based on the mean wave direction, facilitating further analysis in subsequent works.

3.5 Sensitivity Analysis

The sensitivity analysis conducted in this section aims to find out the primary criteria influencing site selection for WEC deployment. Its core methodology involves comparing the number of suitable sites for WEC farm deployment before and after the sensitivity analysis conduction. The computation of this number under the initial conditions is based on the coordinates within a specific area on the map, aligned with the geographic coordinates (longitude: from -19.99 to 44.99, latitude: from 30.00 to 46.99) utilised in the wave datasets employed in previous work.

Under the initial selection criteria condition, 198,541 coordinates have been identified as suitable sites on the final site assessment map. Subsequently, we utilise this count of 198,541 coordinates as the baseline value and normalise the number of coordinates obtained through the sensitivity analysis. This normalisation process enables the quantification of the sensitivity of each selection criterion.

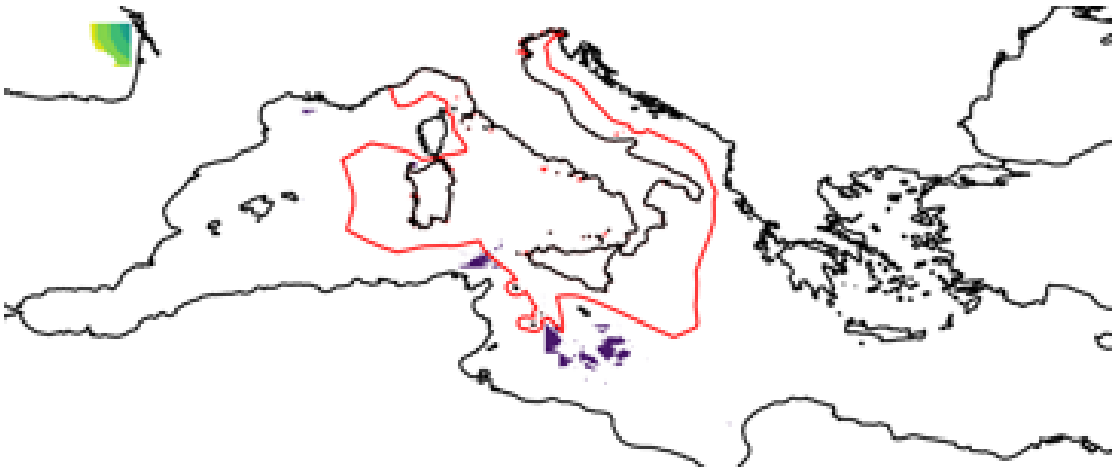

Figure 3.13 Final Site Assessment Map Python

This sensitivity analysis aims to assess how changes in specific criteria affect the outcome of the site selection process for a WEC farm.

In this work, the analysis focuses on the technical sector, with variables including the threshold value of swh, mwp MVI, Accessibility, and Bathymetry. By evaluating these criteria under stricter and looser conditions, with variations of up to 30%, we aim to understand their relative importance and impact on selecting suitable sites for WEC deployment.

Table 3.5 Sensitivity Analysis for Location Selection

Selection Criteria	**Initial Condition**	**Stricter Condition @30%**	**Looser Condition @30%**
Significant Wave Height	[0.5, 4]	[0.65, 2.80]	[0.35, 5.20]
Mean Wave Power	[5, +∞)	[6.5, +∞)	[3.5, +∞)
MVI	The most unstable 40 %	The most unstable 58 %	The most unstable 22 %
Accessibility	[60%, 100%]	[78%, 100%]	[42%, 100%]
Bathymetry	[-300, 0]	[-210, 0]	[-390, 0]

Python processes the new thresholds for sensitivity analysis. *(Code Segment Example is shown in Appendix)*

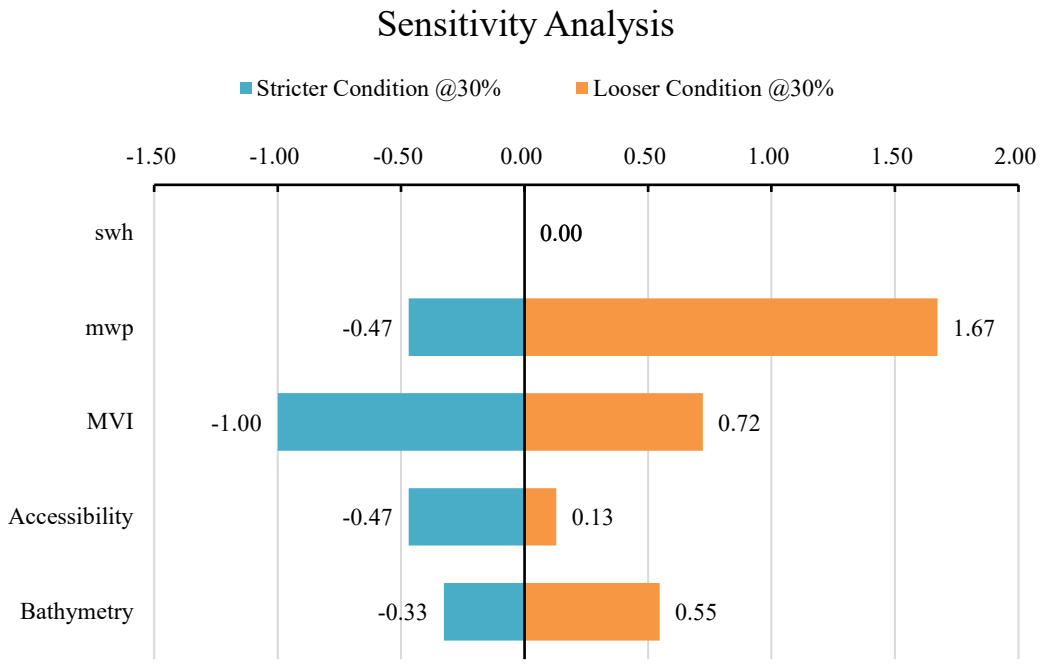

Figure 3.14 Sensitivity Analysis Result for Location Selection

The sensitivity analysis reveals no change in sensitivity (denoted by a value of 0.00) under swh threshold variations. This implies that site assessment remains unaffected by changes in swh thresholds.

However, for mwp threshold variations, under stricter conditions, there is a negative sensitivity value (-0.47), indicating that tightening this threshold reduces the number

of suitable sites. Conversely, the number of suitable sites significantly increases by more than 167% under looser conditions.

The MVI exhibits a substantial negative sensitivity (-1.00) under stricter conditions, indicating that tightening the threshold by 30% results in no existing suitable sites, while under looser conditions, the MVI shows a moderate positive sensitivity (0.72), implying that easing the condition has a relatively positive impact on increasing suitable sites.

Regarding the accessibility thresholds, they indicate a minor negative sensitivity (-0.47) under stricter conditions and a slightly positive sensitivity (0.13) under looser conditions. This suggests that changes in accessibility thresholds impact the number of suitable sites, although not as pronounced as the sensitivity observed for mwp and MVI.

Lastly, bathymetry thresholds have a slight negative sensitivity (-0.33) under stricter conditions and a moderate positive sensitivity (0.55) under looser conditions. This indicates that loosing the bathymetry threshold results in a notable increase in suitable sites, demonstrating a more pronounced impact on site suitability than stricter conditions.

Chapter 4: WEC Annual Energy Production and Array Generation

After completing the site selection process, this chapter delves into the technical aspects of establishing a reference WEC farm. Initially, the focus will be on calculating the annual energy production for a single WEC device, a task contingent upon assessing the device's technical characteristics and the prevailing wave conditions at the chosen site. Subsequently, the methodology for constructing a WEC array will be elucidated. Nonetheless, two preparatory tasks must be addressed before commencing the formal proceedings.

(a) The Geoinformation of the selected site for the WEC farm.

For the site selection map introduced before, geographic grid partitioning was performed in Python based on the spatial resolution of the wave databases.

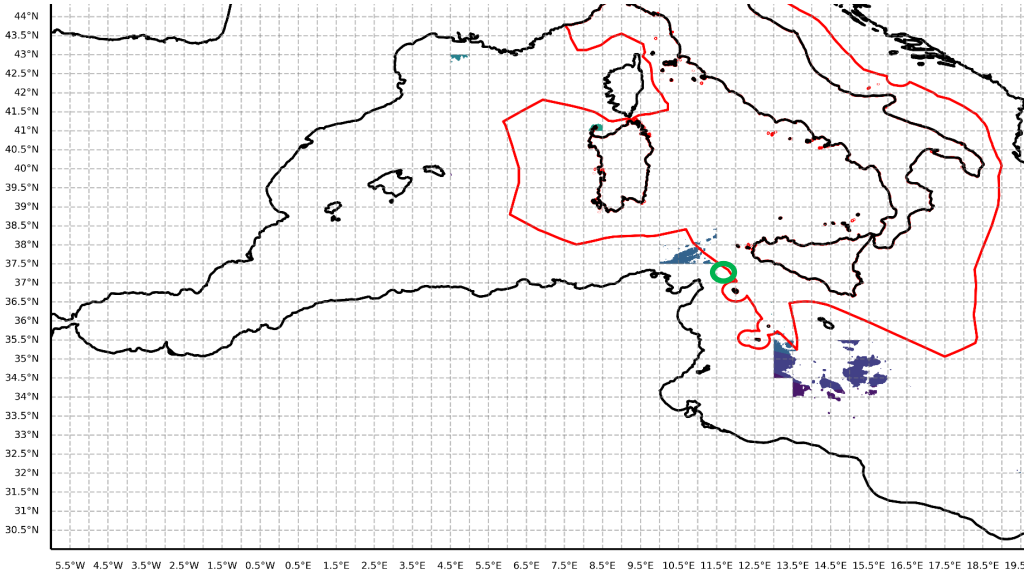

Figure 4.1 Final Site Assessment Map with Geographic Grid In Python

In this thesis work, the selected site is denoted by green circles in the figure, with the approximate site being to the west of Sicily Island.

Table 4.1 Geoinformation for Selected Site

Site	Latitude	Longitude
L1	38° N	11.5° E

(b) The Wave Parameters at the chosen site.

We can retrieve the swh and mwp values for the selected site from the wave databases. Then, based on the linear wave theory and formulas introduced in Chapter 2, The required wave parameters can be calculated. This process is as follows and is implemented via Python. *(Code Segment Example is shown in Appendix)*

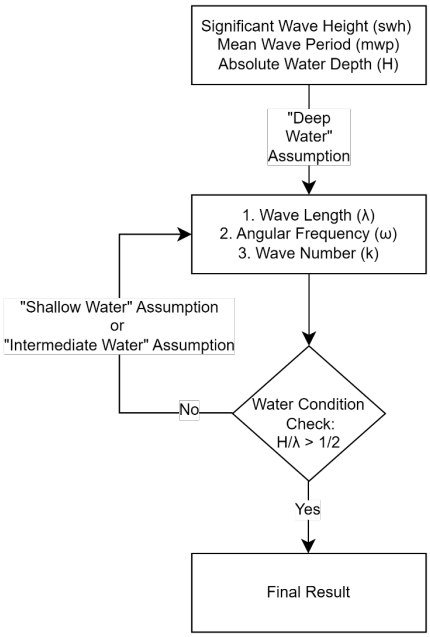

Figure 4.2 Process of Wave Parameters Calculation

Table 4.2 Wave Parameters at The Selected Site

Condition	Mean Condition @2010to2019
Significant Wave Height (m)	1.16
Mean Wave Period (s)	4.98
Absolute Water Depth (m)	100
Wave Length (m)	38.77
Angular Frequency (rad/s)	1.26
Wave Number (rad/m)	0.162

4.1 AEP for a Single WEC

In this section, we will introduce the energy power production of WEC devices. WEC devices generate different output power under varying climatic conditions, such as wind turbines. However, unlike wind turbines, whose power curve depends solely on wind velocity, the power matrix of WEC devices depends on both significant wave height and the mean wave period of the wave, as shown in the figure below.

The power matrix data is obtained from the MOREnergy Lab.

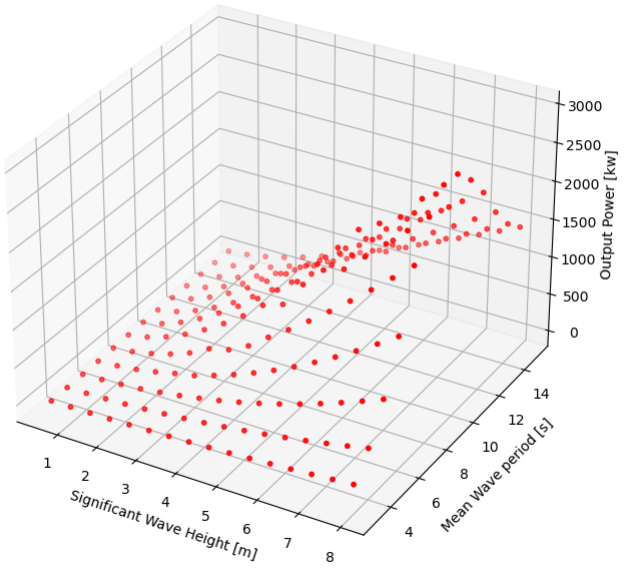

Figure 4.3 Power Matrix of a WEC Device

By correlating the power matrix with the swh and mwp values at the selected site, we can determine the power output for a specific time slice. Then, by accumulating the output power over the entire year, we can calculate the Annual Energy Production of a single WEC device.

Table 4.3 Annual Energy Production for A Single Device

Geo Information	**Device Num**	**AEP (Thesis work)**	**AEP (MORE-EST Platform)**
38° N , 11.5° E	1	660.80 MWh	662.94 MWh

The table presents the Annual Energy Production values obtained in this thesis work alongside the values generated by the MORE-EST Platform for the same site. There is a 0.3% discrepancy between the two sets of values, which could be attributed to systematic errors in the calculation process.

4.2 WEC Array Generation

Real energy projects are expected to use device arrays instead of individual devices for power generation, as seen in wind farms, solar photovoltaic fields, etc. This array approach can offer several advantages, including:

(a) Increased Power Output: Device arrays can aggregate energy captured from multiple devices, resulting in higher power output than individual devices.

(b) Improved System Reliability: Operating multiple devices within an array can provide redundancy in case of one or more device failures, thereby enhancing system reliability.

(c) Cost-effectiveness: Although the initial investment for deploying multiple devices is higher than for a single device, the array's increased power output and reliability can lead to long-term energy production and maintenance cost savings.

For wave energy farms, there is an additional advantage known as the “constructive park effect”, as mentioned in Chapter 2, which arises from the wave propagation characteristics and the energy capture mechanism of WECs, especially the point absorbers, suggesting that deploying WECs in an array may ultimately yield higher power outputs than expected.

Considering the advantages mentioned, this section will introduce a method of building a WEC array. In the literature review, many researchers have discussed the WEC array construction and provided some guiding principles for designing an optimal array configuration.

Ricci et al. [95] proposed that the distance between devices should be greater than four times the device radius for point absorber arrays in Portuguese wave conditions. On the other hand, Sharp suggested that the minimum spacing between devices in an array should be six times the device radius. Bozzi et al. [34] utilised BEM software to propose the optimal arrangement of point absorber arrays in Italian wave conditions as rhombus-shaped, with an optimal spacing ranging from 20 to 40 times the device radius, while Engström et al. [96] suggested that a rectangular array is a more efficient configuration, for Swedish sea conditions.

Several former recommendations have been incorporated into this work for designing the WEC array. The relevant array parameters are outlined in the table below:

Table 4.4 WEC and Array Parameters

Parameter	**Name in Codes**	**Value or Range**	**Unit**
Device Num	target_WECs_num	10	/
Num of Rows for the Array	target_row_num	1 or 2 or 3	/
Device Radius	WEC_radius	4	Meter
Offset Angle	offset_angle_values	(0, 45)	Degree
Distance in X-axis	distance_x_values	(2 * WEC_radius, 20 * WEC_radius)	Meter
Distance in Y-axis	distance_y_values	(2 * WEC_radius, 20 * WEC_radius)	Meter

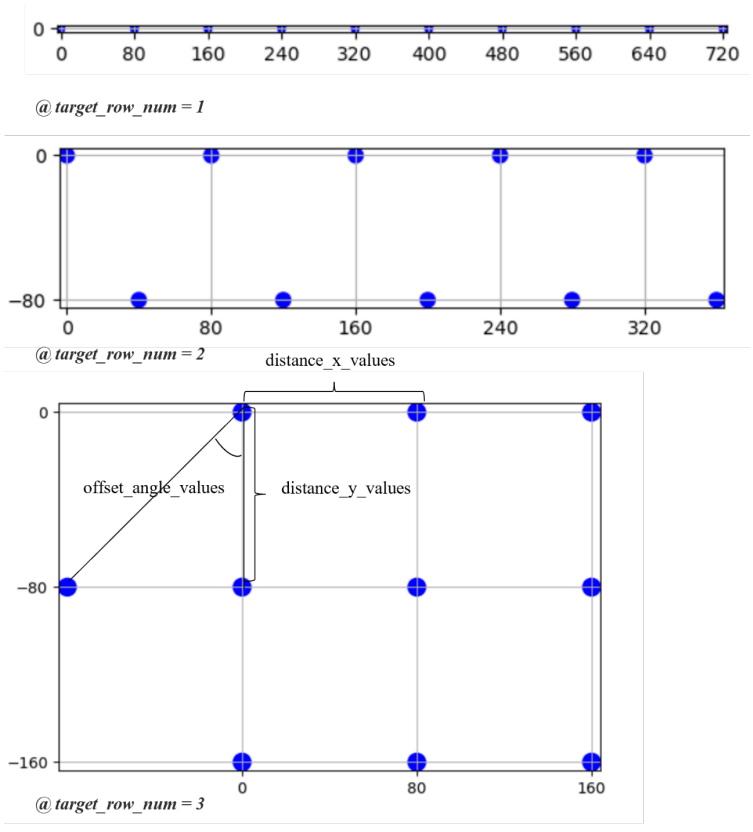

Figure 4.4 Schematic diagram for A WEC Array

The figures above show that the specific WEC array can be generated via Python based on the array parameters. These figures depict the array structures for row numbers equal to 1, 2, and 3, respectively, and the array structures for offset angles of 0 degrees, 27.5 degrees, and 45 degrees.

Wave direction is widely recognised as a crucial characteristic parameter of waves. Faraggiana et al. [97] proposed that WEC performance is sensitive to wave direction. Additionally, through BEM simulations, Zhiwen Wei et al. found that wave direction directly influences the WEC performance and corresponding control strategies. Sinha et al. [98] also indicated in 2016 that array configuration is directly related to wave direction, with different wave directions corresponding to different optimal array configurations.

In this thesis work, the angle between the wave direction and the Y-axis of the WEC array is defined as the "Wave Angle." For the WEC array, the wave is expected to be the head sea, necessitating a global deviation angle for the entire array to match this requirement. This global deviation angle is determined based on the wave direction at the selected site, which may vary with site changes. To facilitate the placement of arrays within the chosen site while ensuring a proper global rotation, an automated identification code has been developed in Python.

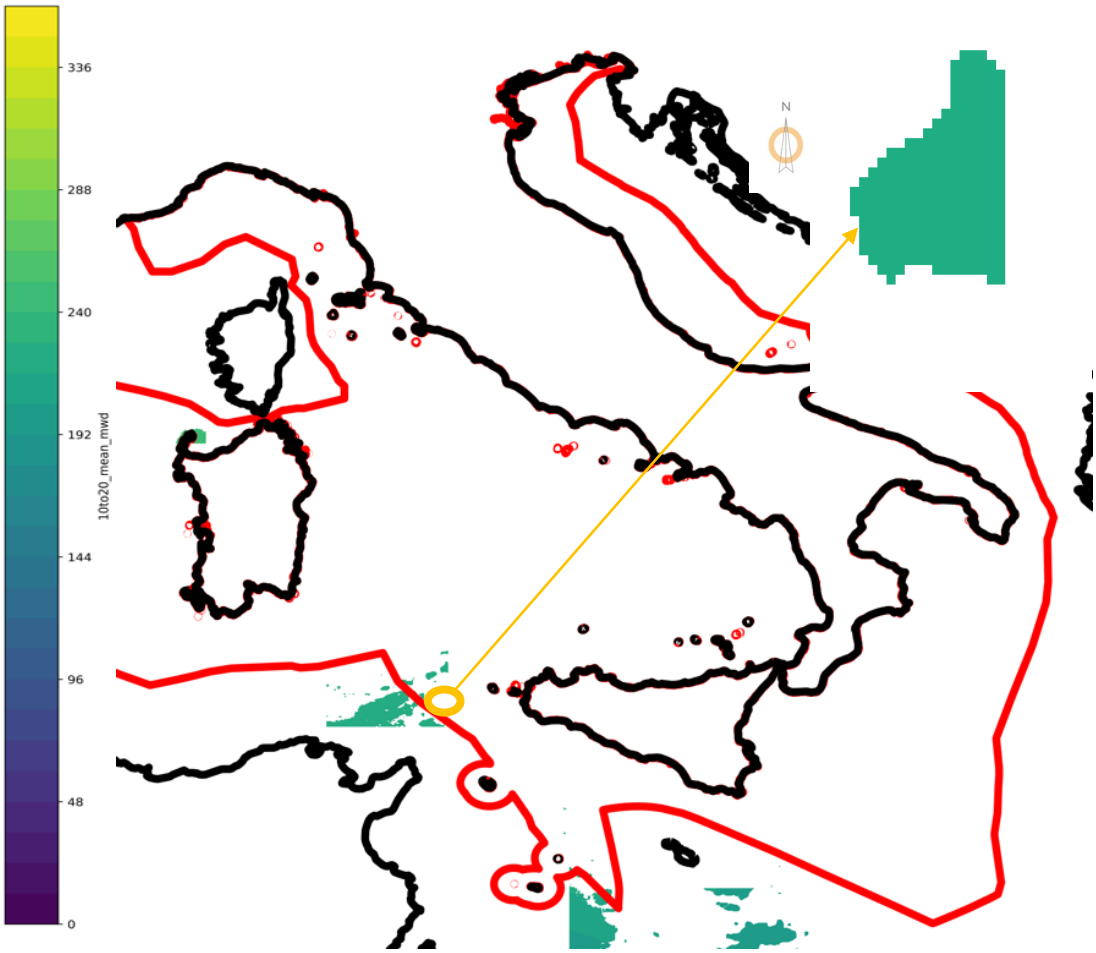

Figure 4.5 Site Shape Extraction In Python

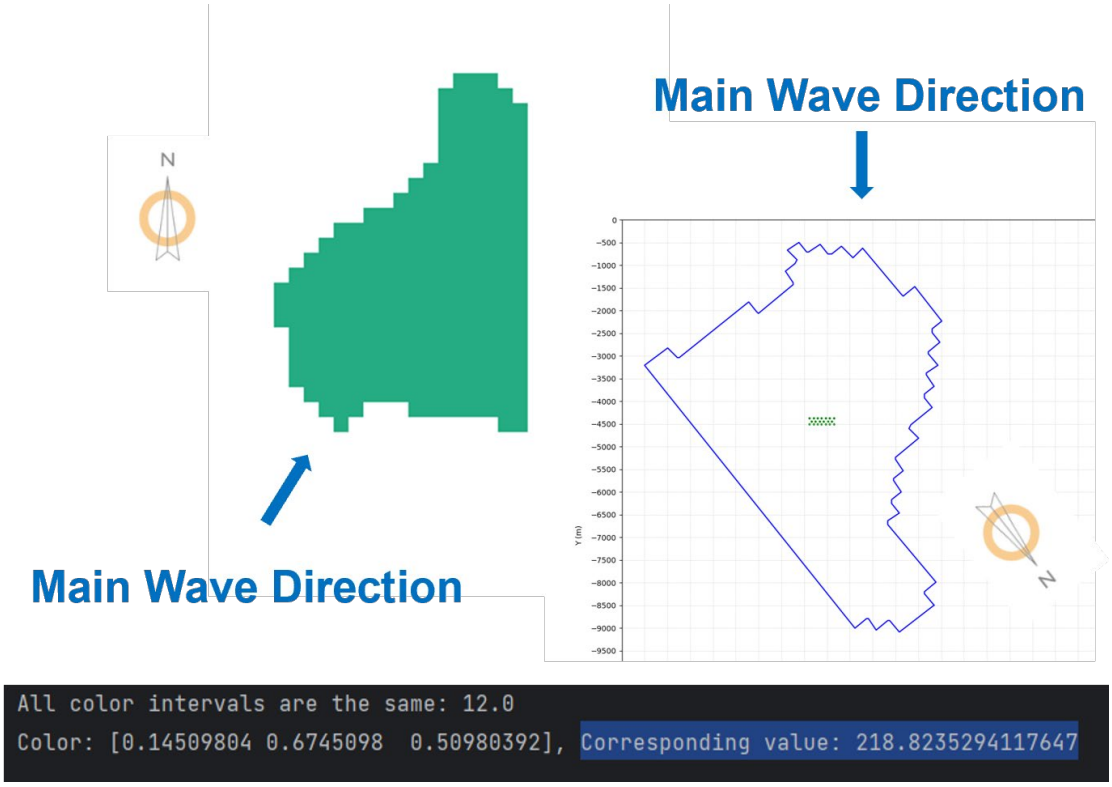

Figure 4.6 Array Auto-generation In Python

As illustrated in the figure, the code can automatically identify and generate the outline of the selected site. It then positions the array at the centre of the outline and, based on the colour values of pixels within the region, matches the mwd defined by the colour bar. Finally, it applies a bias rotation to the outline to align it with the corresponding mean wave direction of the current region.

Chapter 5: WEC Array Optimisation

As outlined in the preceding chapter, WEC arrays offer advantages such as Increased Power Output and enhanced Cost-effectiveness. In this chapter, we will conduct a technical analysis and economic analysis of a WEC array comprising ten devices. We will investigate the impacts of interaction between WECs in various configurations and explore a particular configuration that maximises technical and economic factors.

Before proceeding with the formal work, some validation tasks need to be completed to ensure the accuracy of subsequent efforts.

(a) Code Validation:

In Chapter 2, we discussed the Point Absorber Approximation to study interactions within the array and quantify this effect by the q factor. The following work in this section is based on this analytical theory, implemented in Python.

The primary process is as follows:

Build a WEC array.

1. Compute the required wave parameters from the wave databases.
2. Utilize formulas introduced in Chapter 2 to calculate the q factor of the array under specific wave conditions.
3. Determine the optimal array configuration in terms of the offset angle, distance in the x-axis, and distance in the y-axis, i.e., the values of these three variables when the q factor is maximised.

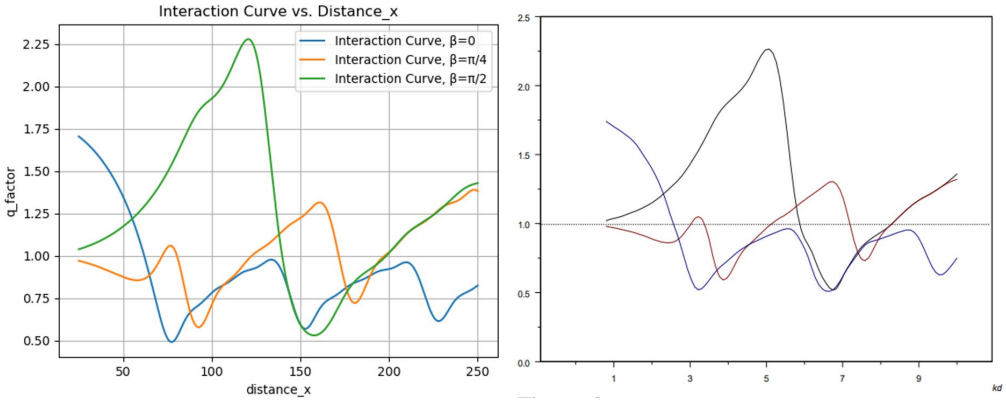

Figure 5.1 Code Check (the right one is generated in this work, and the left one is from Ref. [99])

(b) Theory Check:

Having confirmed the correctness of the code, the next step is to validate the Point Absorber Approximation to describe the interaction effects within the array accurately.

Some researchers have already demonstrated its usability, such as Göteman et al., who [100] compared q-factor results generated by Point Absorber Approximation with those from WAMIT, and she indicated that the approximate model exhibits good agreement with the numerical method for small parks. Here, we validate it under the condition of "infinite distance" on the x-axis. Ideally, when the distance between devices in the x-axis is "infinite," they would be considered isolated devices rather than in the array. Therefore, the q factor of this "infinite distance" array condition should be 1, indicating no interaction effect within the variety.

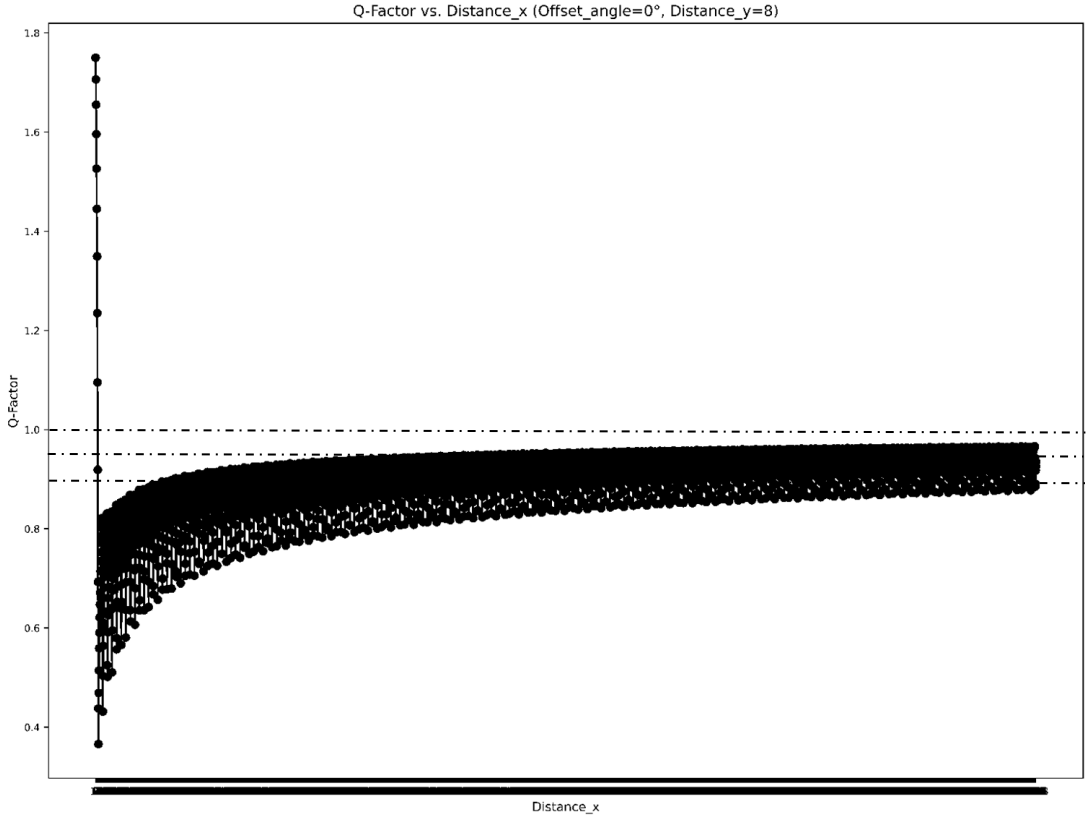

Figure 5.2 Point Absorber Approximation Validation

The figure above shows that the q factor quickly approximates to around 0.95 under the "infinite distance" array condition, reaching approximately 0.975 ultimately when "Distance = 1250 times the Radius." Subsequent validation of the "infinite distance" data is not feasible due to limitations in laptop performance, but 0.975 is considered acceptable.

5.1 Technical and Economic Optimisation for an Array at Fixed k

WEC device power output has been repeatedly indicated as directly correlated with wave conditions in former chapters. This section will examine the array's performance under specific wave conditions and conduct technical and economic assessments accordingly.

The corresponding input parameters are as follows, and the wave number (k) will be utilised as a characteristic parameter to describe the wave conditions, in the codes.

Table 5.1 Parameters for Technical Assessment

Parameter	Name in Codes	Value or Range	Unit
Wave Number	k	0.162 @ mean condition	rad/m
Significant Wave Height	swh	1.16	Meter
Angular Frequency	omega	1.26	rad/s
Wave Length	lamb	38.77	m
Device Radius	a	4	Meter
AEP of a Single Device	annual_energy_production_single	660.80	MWh
Wave Angle	beta	0	Degree
Water Density	rho	1,000	kg/m3
Gravity Acceleration	g	9.8	N/kg
Absolute Water Depth	H	10	Meter

(1) The calculation process of wave parameters has been mentioned in Chapter 4. For further details, please refer to that chapter.
(2) The way to calculate Annual Energy Production for a Single Device has been introduced in Chapter 4. For further details, please refer to that chapter.

Considering that Reference [41] [42] mentions the mathematical assumption of the point absorber approximation being valid when 'ka'$\leqslant$0.8, as mentioned in Chapter 2. As you can see, based on the data in the table, the 'ka' in this work is approximately 0.64, which is below the threshold of 0.8.

The above are the relevant parameters for technical assessment, and the parameters for economic assessment are as follows:

Table 5.2 Parameters for Economic Assessment

Parameter	Name in Codes	Value or Range	Unit
Device Rated Power	Rated_power	500	kW
PTO	PTO_type	Hydraulic / Linear generator / Mechanical / Air turbine	/
Structure	Structure	Mooring / Foundation	/
Mooring Chain	chain_type	Stud-link chain / Studless chain	/
Diameter of the Chain	Diameter_line	90	mm
In-array Cable Voltage	Voltage_MAC	11	kV
Export Cable Voltage	Voltage_HAC	33	kV
In-array Cable Length	Length_cable_inner	Auto-Calculated	Meter
Export Cable Length	Length_cable_export	10,806	Meter
Decommission Factor	decommission_factor	0.88	/
USD to EUR	USD_to_EUR_exchange_rate	0.93 @2023.Dec	/
Discount Rate	discount_rate	0.04	/
Project Lifetime	project_lifetime	20	Years
Project State	stage_state	Single_Device / Small_Array / Utility_Scale / High_Maturity	/

(1) The parameters serve as input variables, allowing users to customise the economic analysis of the array according to their requirements.
(2) The inputs for PTO, Structure, Mooring Chain, and Project State are string types, and the code will execute different calculations based on the specific strings provided. For further details, please refer to the economic model outlined in Chapter 2.
(3) The In-array Cable Length is automatically calculated based on the generated array configuration and does not require user input.

Another thing that needs to be mentioned is the Export Cable Length parameter. Considering the proximity of our selected site for the WEC array to an ongoing offshore wind farm project, "Med Wind Project", and in alignment with economic considerations, it was assumed that the export cable of our array would be directly connected to that existing project rather than directly to the shore.

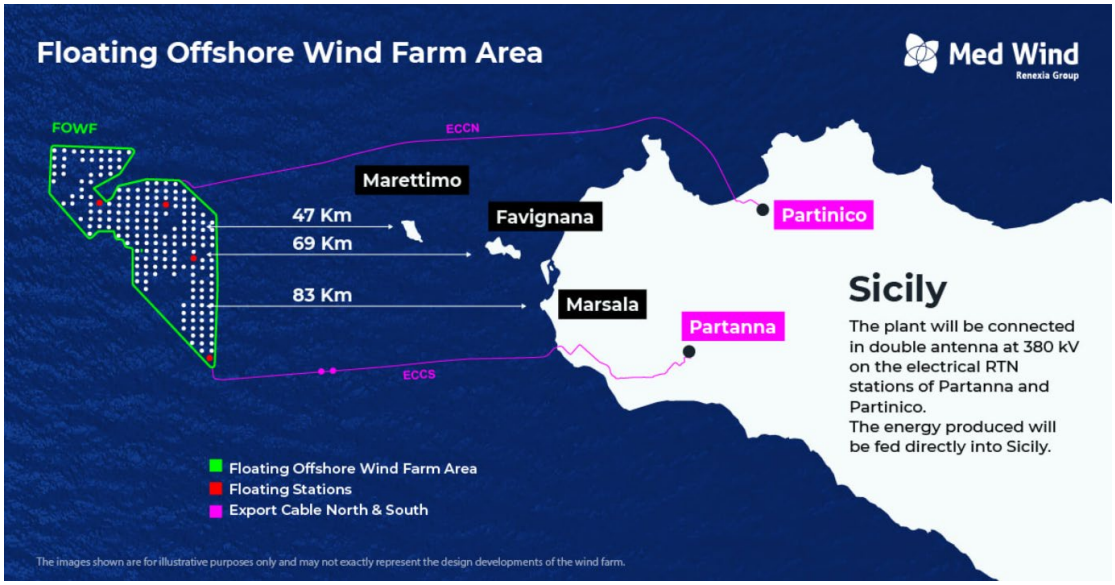

Figure 5.3 Med Wind Project

To determine the length of the export cable (the straight-line distance from our array to the "Med Wind Project"), we mapped the approximate orientation and outline of the latter onto the site selection map in QGIS, as illustrated in the figure below. Finally, distance measurement tools were utilised to ascertain the distance.

Figure 5.4 Med Wind Project Mapped In QGIS

Now, we have all the required parameters and can formally proceed with the technical and economic assessment of the array.

5.1.1 Single-row Array

Firstly, we will consider a single-row array with 10 WECs and attempt to find the optimal array configuration under the technical and economic assessment.

(a) Technical Assessment

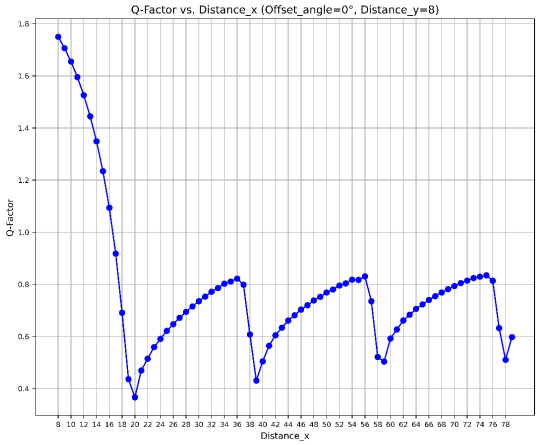

Figure 5.5 q factor VS Distance in X Axis for Single-row Array @ Fixed k

From the figure, we can observe that the q factor of the array fluctuates as the distance between devices within the array increases, with the magnitude of fluctuations gradually decreasing over the range. The maximum q factor undoubtedly occurs at the minimum distance between devices, where the spacing is 2 times the device radius, yielding a q-factor of 1.749, capable of generating significant constructive park effects with the AEP for an array equal to 11563.16 MWh. However, at this point, there may be considerable displacement of devices due to the extreme proximity.

Then, we can calculate each device's displacement using the equations and theories introduced in Chapter 2 to verify whether the array structure at the maximum q factor meets the displacement requirement.

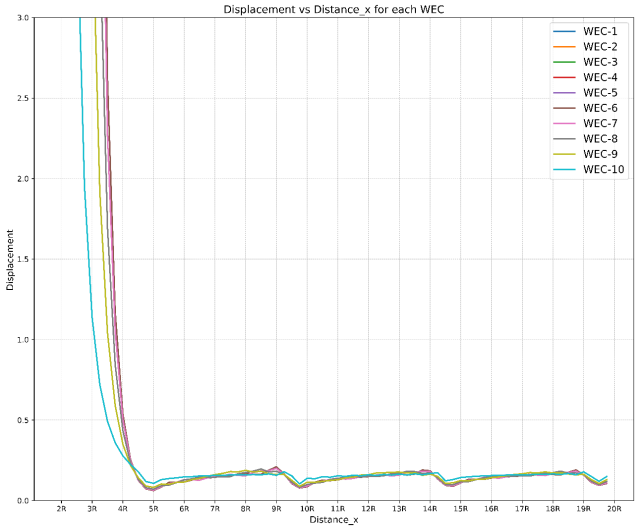

Figure 5.6 Displacement of Each Device VS Distance in X Axis for Single-row Array @ Fixed k

Under the configuration with the maximum q factor of 1.749 (where the spacing is equal to 2 times the device radius), the dimensionless displacement vector of some devices in the array exceeded the dimensionless threshold of 3. Hence, this configuration was deemed unsuitable. However, to satisfy the displacement constraint, the array configuration with the maximum q factor should have a device spacing of 3.5 times the device radius, with a q factor of 1.348 and the AEP for the array equals 8913.62 MWh. Under this configuration, the interaction of devices within the array will exhibit constructive park effects.

(b) Economic Assessment

In the economic analysis, the assessment factor will be the LCoE, whose formula and calculation process have been described in the economic model section of Chapter 2. Here, we will focus on discussing the performance of the array.

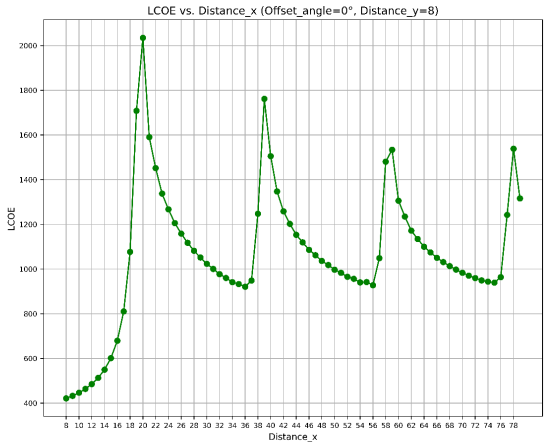

Figure 5.7 LCoE VS Distance in X Axis for Single-row Array @ Fixed k

As shown in the figure, the LCoE of the array also shows a fluctuation trend with the increase in device spacing and exhibits a pattern of diminishing fluctuations with the increase in spacing. In terms of correlation, there is an approximately inverse relationship between LCoE and the q factor. This is because the change in cost appears negligible relative to the change in q factor (or AEP of the array) concerning the array configuration changing, resulting in the techno-economic indicator LCoE being directly correlated with the technical factor (AEP).

Similarly, the optimal array structure with a spacing of 8 meters, two times the device radius, yields an LCoE of 421.54 EUR/MWh. However, considering the displacement

constraint, the optimal array structure should change to a spacing of 14 meters (3.5 times the device radius), with an LCoE of 549.92 EUR/MWh.

5.1.2 Two-row Array

The difference between a multi-row array construction and a single-row array construction is that more than one element affects the array configuration. Specifically, as mentioned in Chapter 4, an array configuration involves three components: the offset angle, distance in the x-axis, and distance in the y-axis. For a single-row array, the useful element is only the distance in the x-axis. However, all three elements come into play for a multi-row array.

(a) Technical Assessment:

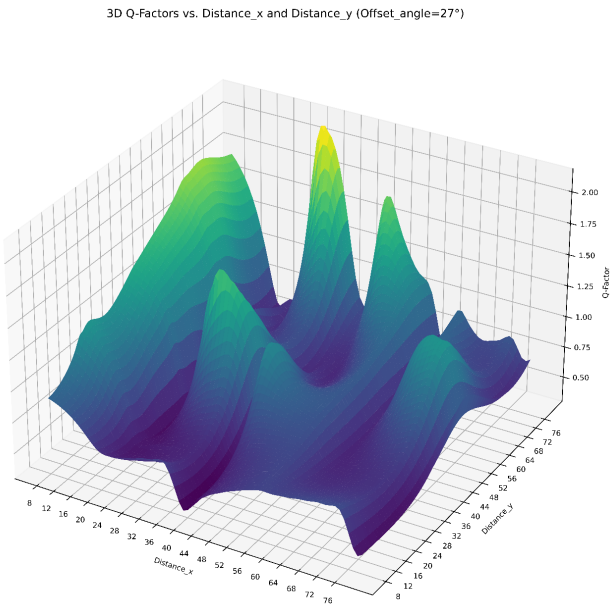

Figure 5.8 q factor VS Distance in X Axis for Two-row Array @ Fixed k

The above figure illustrates the three-dimensional variation of the q-factor with respect to the distance in the x-axis and the y-axis, based on the optimal array configuration with a fixed offset angle of 27 degrees, which is one of three elements of the optimal array configuration. Then, from the figure, we can read that the other two elements of the optimal array configuration are 31 meters (7.75 times the device radius) at a distance in the X-axis and 78 meters (19.5 times the device radius) at a distance in the Y-axis.

The q factor under this configuration is 2.142, with the AEP for the array of 14156.01 MWh. The schematic diagram of the array configuration is shown below.

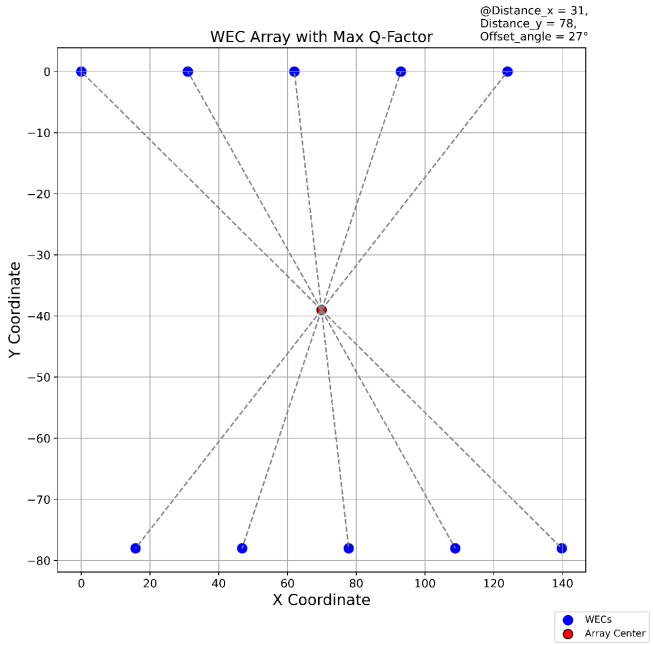

Figure 5.9 Schematic Diagram for The Two-row Array with Optimal Configuration

Similarly, we can calculate the displacement vector for each device in the array to determine whether the current optimal array configuration satisfies the displacement constraint.

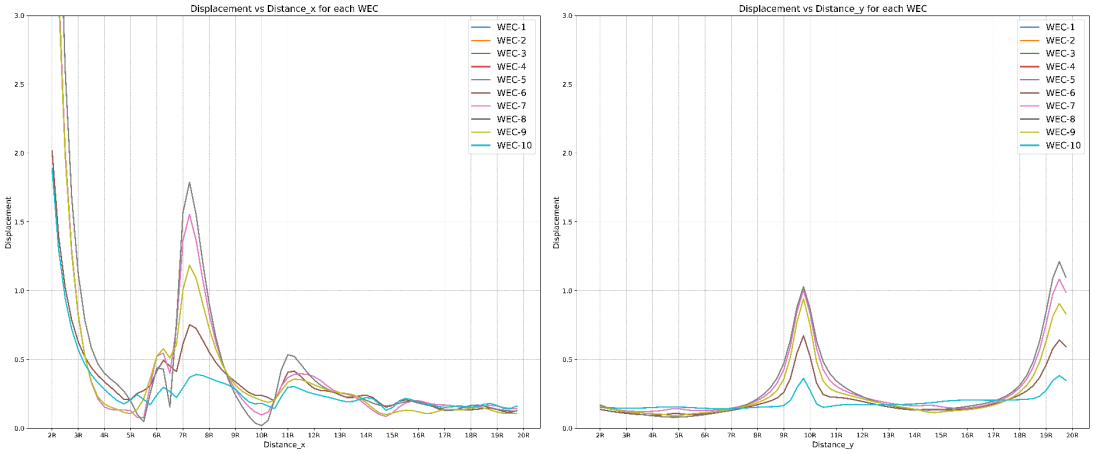

Figure 5.10 Displacement of Each Device VS Distance in X and Y Axis for Two-row Array @ Fixed k

From the graph, it can be observed that the current optimal array configuration fully satisfies the displacement constraint.

(b) Economic Assessment:

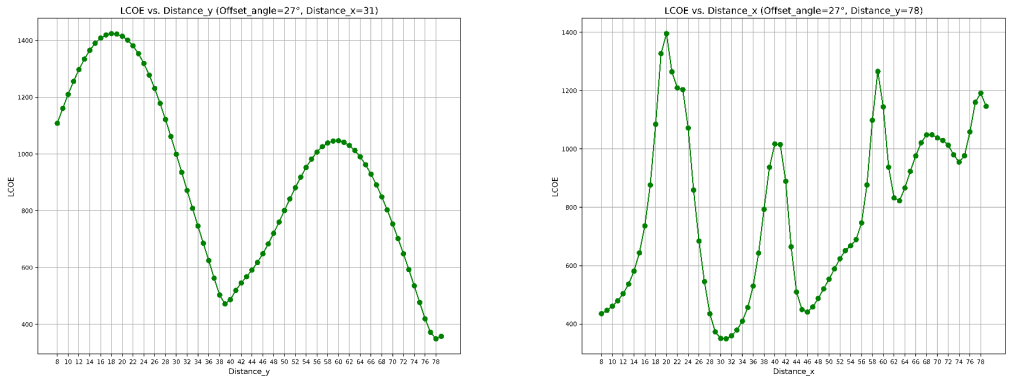

Figure 5.11 LCoE VS Distance in X and Y Axis for Two-row Array @ Fixed k

For the economically optimal array configuration, we can see that it remains the same as the technically optimal array configuration, with three elements: an offset angle of 27 degrees, a distance of 31 meters (7.75 times the device radius) in the X-axis, and a distance of 78 meters (19.5 times the device radius) in the Y-axis. At this configuration, the array's LCoE equals 349.15 EUR/MWh.

5.1.3 Three-row Array

The three-row array, like the two-row array, belongs to the category of multi-row arrays. Its array configuration consists of three elements: the offset angle, distance in the x-axis, and distance in the y-axis.

(a) Technical Assessment:

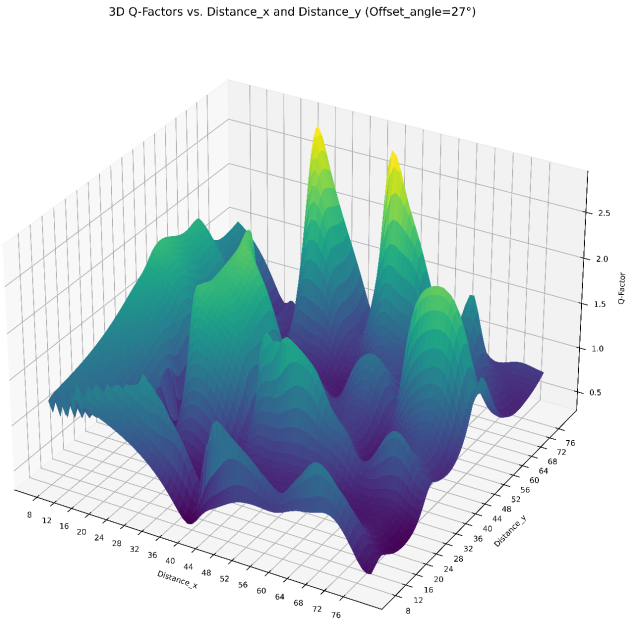

Figure 5.12 q factor VS Distance in X Axis for Three-row Array @ Fixed k

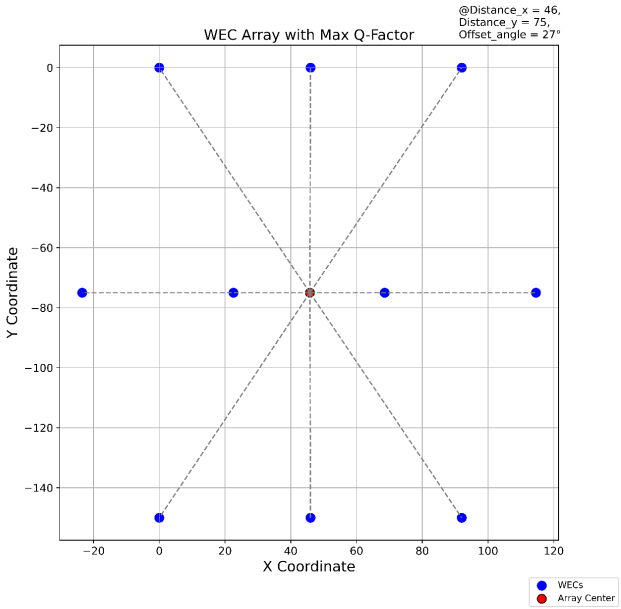

Figure 5.13 Schematic Diagram for The Three-row Array with Optimal Configuration

From the graph, we can see that similar to the optimal configuration for the two-row array, the optimal configuration for the three-row array has an offset angle of 27 degrees. As mentioned in the reference, this may demonstrate that a rhombus formation may be relatively advantageous for some simple multi-row array configurations under the head sea condition.

At this point, the distance in the x-axis is 46 meters, equivalent to 11.5 times the device radius, and the distance in the y-axis is 75 meters, equivalent to 18.75 times the device radius. The q factor is 2.886, and the AEP for the array is 19074.84 MWh. This configuration also meets the displacement constraint.

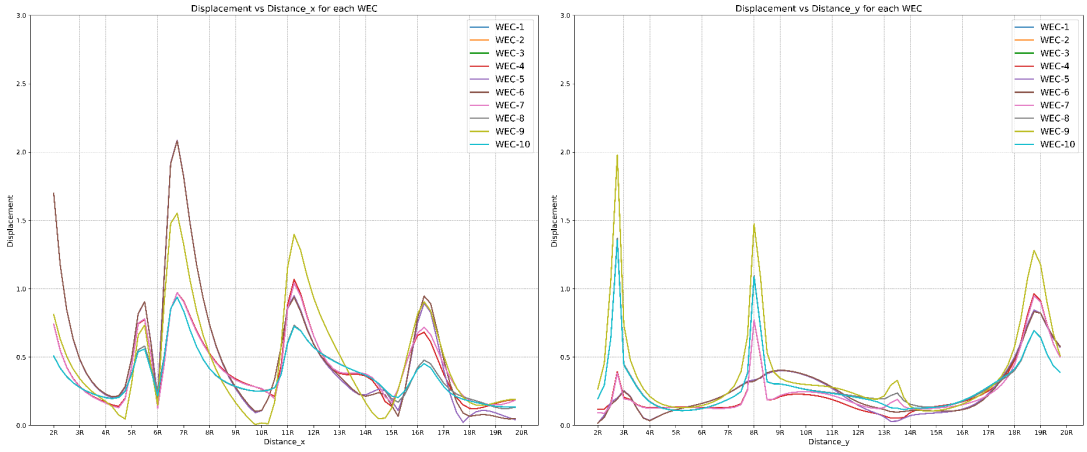

Figure 5.14 Displacement of Each Device VS Distance in X and Y Axis for Three-row Array @ Fixed k

(b) Economic Assessment:

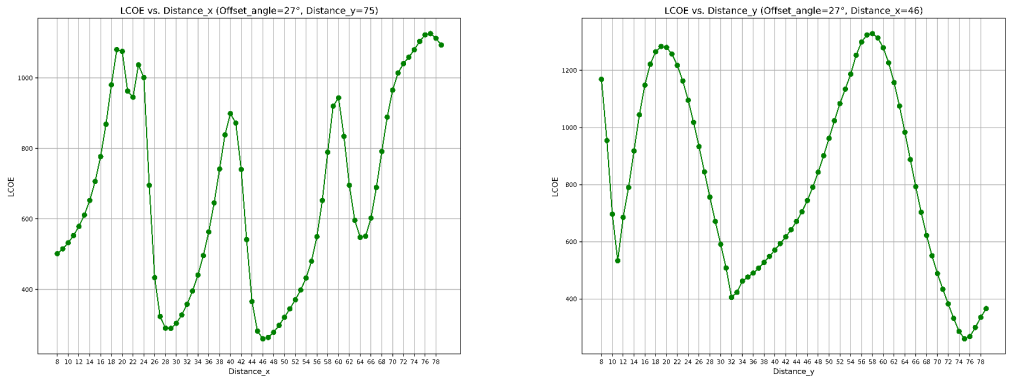

Figure 5.15 LCoE VS Distance in X and Y Axis for Three-row Array @ Fixed k

The optimal array configuration in terms of technical analysis is also the best choice in economic terms. In this configuration, the LCoE for the array is 260.19 EUR/MWh.

5.1.4 Comparison

As we have completed the technical and economic assessment of single-row, two-row, and three-row arrays under fixed wave conditions with a mean wave number k from 2010 to 2019 at a specific selected site, we will further compare them in this sub-section.

Table 5.3 Technical and Economic Assessment For WEC Arrays

	Parameter	**Single-row Array**	**Two-row Array**	**Three-row Array**
	Device Num		10	
	Device Radius (a)		4 meters	
Without the Displacement Constraint	Offset Angle	0 degrees	27 degrees	27 degrees
	Distance in the X-	2a meters	7.75a meters	11.5a meters
	Distance in the Y-	0 meters	19.5a meters	18.75a meters
	q Factor	1.749	2.142	2.886
	AEP of the Array	11563.16 MWh	14156.01 MWh	19074.84 MWh
	LCoE	421.54EUR/MWh	349.15EUR/MWh	260.19EUR/MWh
With the Displacement	Offset Angle	0 degrees	27 degrees	27 degrees
	Distance in the X-	3.5a meters	7.75a meters	11.5a meters

Constraint	Distance in the Y-	0 meters	19.5a meters	18.75a meters
	q Factor	1.348	2.142	2.886
	AEP of the Array	8913.62	14156.01 MWh	19074.84 MWh
	LCoE	549.92	349.15EUR/MWh	260.19EUR/MWh

We can observe that with an increase in the number of rows in the array, the optimal q-factor and AEP of each array increase while the LCoE decreases accordingly. Additionally, except for the single-row array, the optimal configuration of multi-row arrays is not constrained by device displacement conditions.

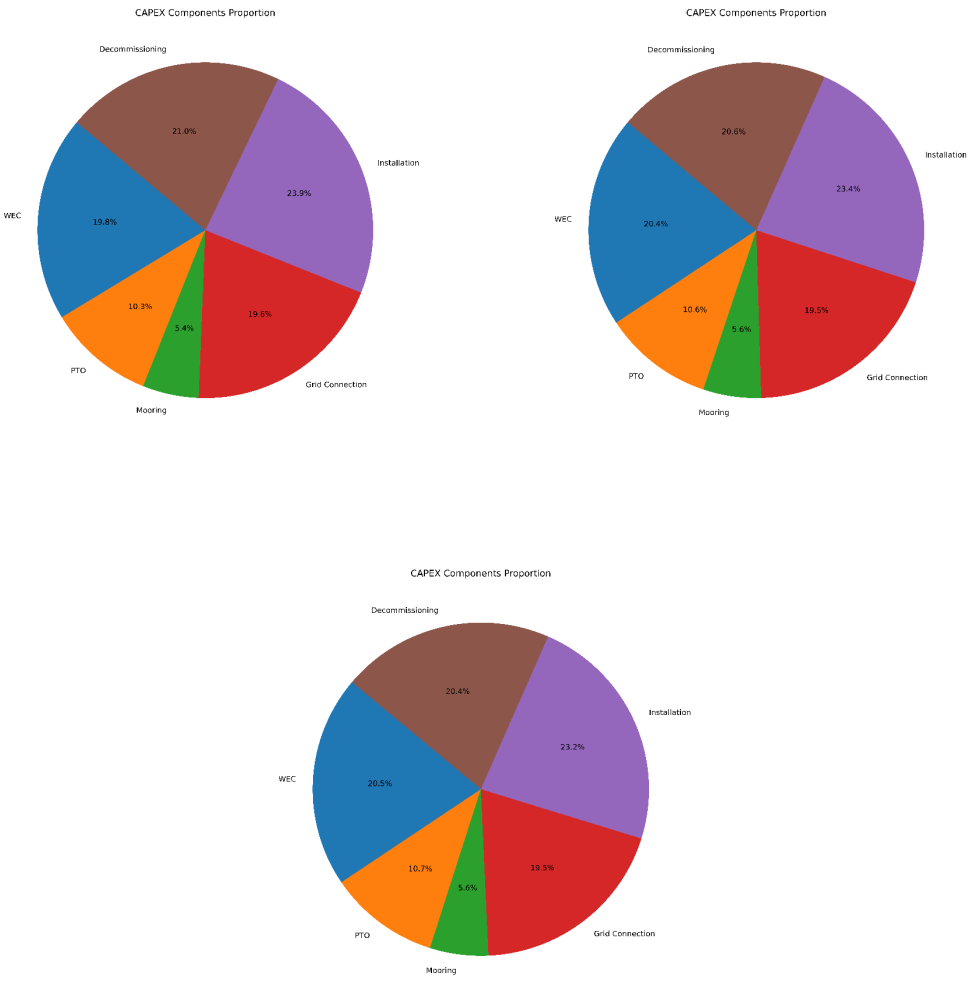

Figure 5.16 Distribution of CAPEX for Single-row, Two-row, and Three-row Array

Table 5.4 Distribution of CAPEX for Single-row, Two-row, Three-row and Reference Array

Elements	**Single-row Array**	**Two-row Array**	**Three-row Array**	**Reference** [47]
Devices	19.8 %	20.4 %	20.5 %	31 %
PTO	10.3 %	10.6 %	10.7 %	22 %
Mooring or Foundation	5.4 %	5.6 %	5.6 %	6 %
Grid Connection	19.6 %	19.5 %	19.5 %	/
Installation	23.9 %	23.4 %	23.2 %	18 %
Decommissioning	21.0 %	20.6 %	20.4 %	
O&M	/	/	/	17 %
Others	/	/	/	16 %
Total CAPEX	100 %	100 %	100 %	100 %

The figure shows that the number of rows in the array does not significantly affect the distribution of elements in CAPEX. According to references [47], the economic analysis conducted in this study aligns well with other projects.

5.2 Technical and Economic Optimisation for an Array at Real k

The previous section's technical and economic analyses were based on a fixed wave condition where the wave number k was constant and equal to the mean value from 2010 to 2019. However, in reality, wave conditions vary in time, and using an average wave condition may not accurately capture the true wave characteristics of the selected site. Therefore, in this section, we will replace the fixed wave number k with a dataset representing wave conditions over a year, with a temporal resolution of 1 hour, corresponding to the wave database.

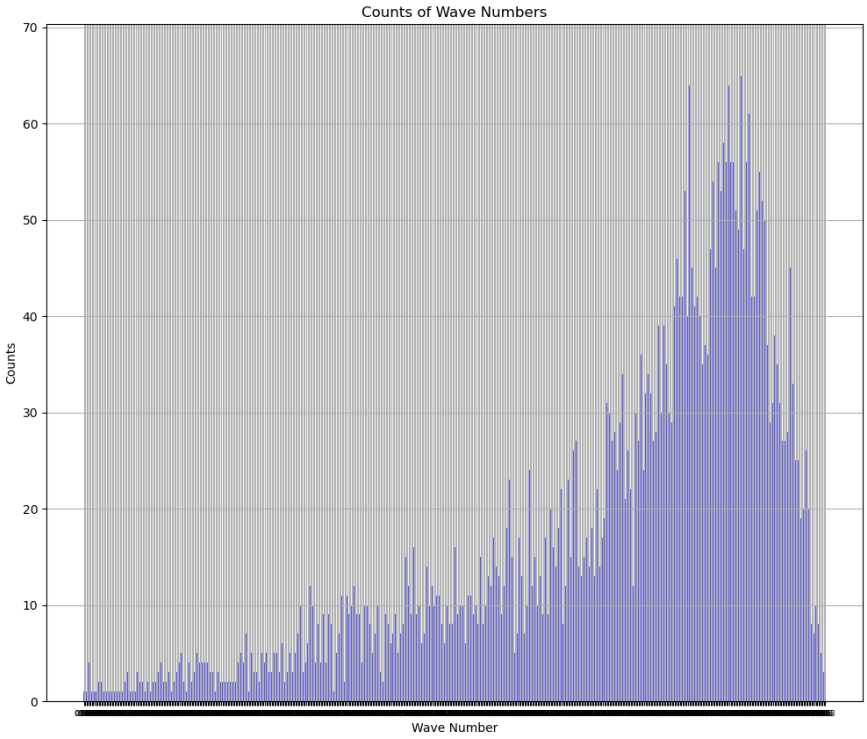

Figure 5.17 Wave Number Counts Plot

The figure above depicts the distribution of wave numbers over a year. All other parameters remain consistent with those used in the previous section.

5.2.1 Single-row Array

(a) Technical Assessment:

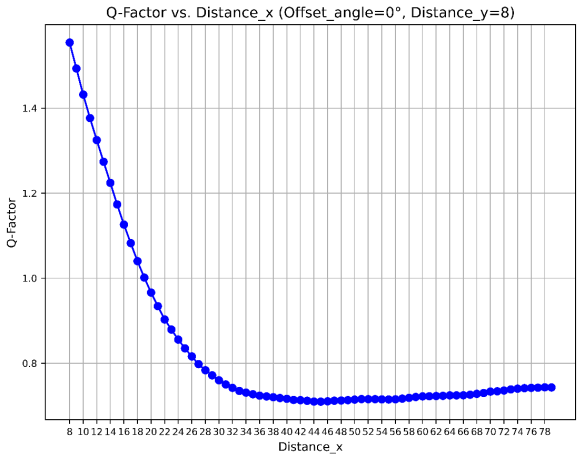

Figure 5.18 q factor VS Distance in X Axis for Single-row Array @ Real k

Due to the use of a real and widely distributed wave number instead of that fixed to the average, the trend graph of the q-factor against the distance in the X-axis for the optimal array configuration shows a more uniform pattern, devoid of the previous fluctuations, and the magnitude of the q factor tends to normalise. However, the optimal array configuration still lies in the scenario with the smallest spacing between devices. The q factor is 1.554, with the AEP of the array equal to 10271.71 MWh.

(b) Economic Assessment:

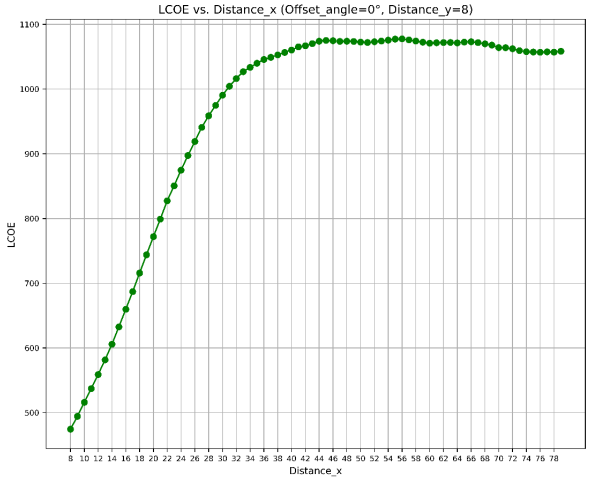

Figure 5.19 LCoE VS Distance in X Axis for Single-row Array @ Real k

The LCoE against the distance in the X-axis figure exhibits a similar trend, albeit in reverse, as lower LCoE values are preferable. Under the optimal array configuration, the LCoE is 474.54 EUR/MWh.

5.2.2 Two-row Array

(a) Technical Assessment:

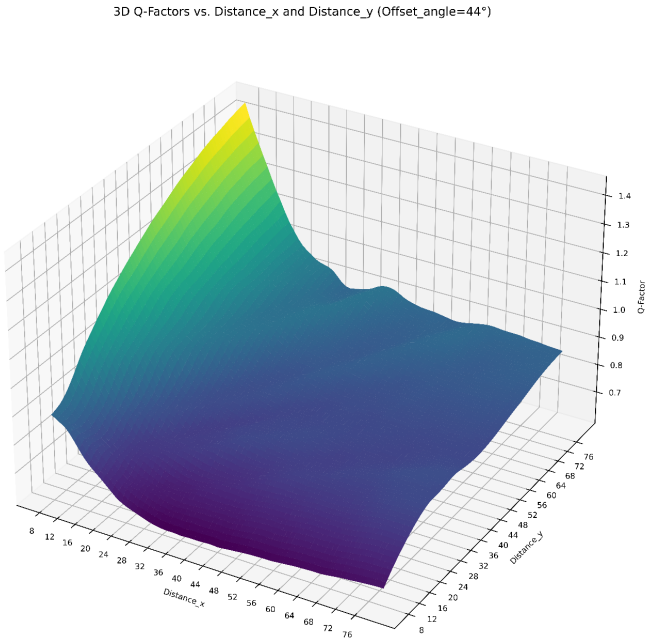

Figure 5.20 q factor VS Distance in X and Y Axis for Two-row Array @ Real k

The code identified the optimal array configuration with one of the elements: offset angle equals 44 degrees, which differs from the fixed wave number k condition, under which we said the rhombus might be the best configuration. Meanwhile, when fixing the offset angle at 44 degrees, studying the variation of the q factor with the distance in the x-axis and the distance in the y-axis revealed a generally monotonic trend with minor fluctuations.

The optimal array configuration is with an offset angle of 44 degrees, a distance in the x-axis of 8 (2 times the device radius), and a distance in the y-axis of 79 (19.75 times the device radius). The q factor is 1.447, and the AEP for the array is 9562.39 in this condition.

(b) Economic Assessment:

Similarly, the optimal array configuration for economic analysis is the same as in technical analysis, with an LCoE of 513.80 EUR/MWh. The following figure shows this optimal configuration.

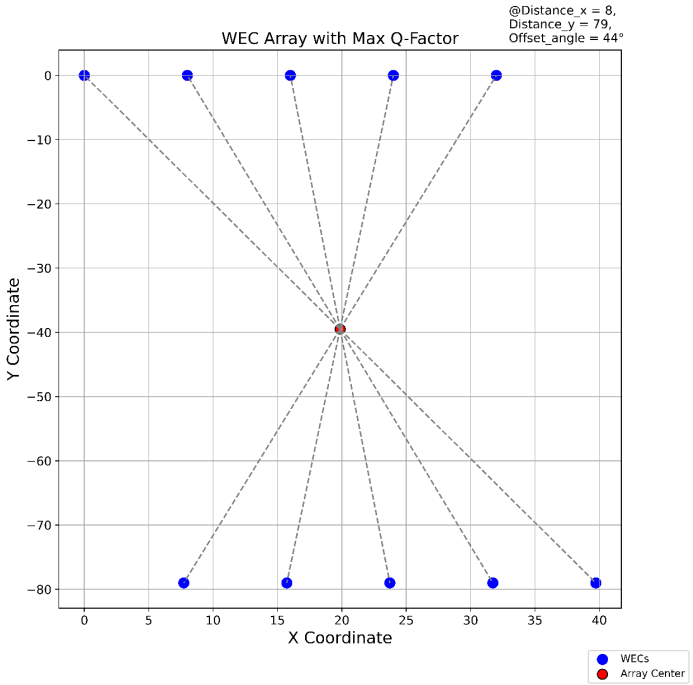

Figure 5.21 Schematic Diagram for The Two-row Array with Optimal Configuration

5.2.3 Three-row Array

(a) Technical Assessment:

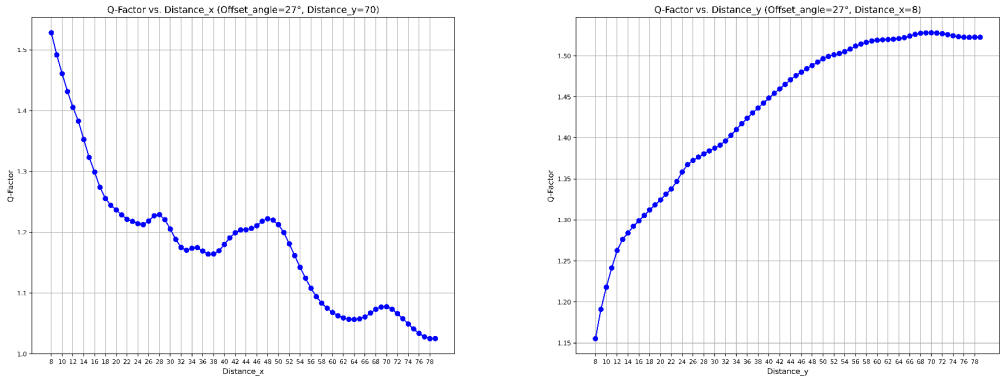

Figure 5.22 q factor VS Distance in X and Y Axis for Three-row Array @ Real k

Regarding technical optimisation, the optimal array configuration exhibits a degree of similarity to the configuration identified under fixed wave number k conditions. Specifically, the rhombus arrangement is optimal for the three-row array even under actual wave number scenarios. The remaining two parameters, the distance in the x-axis and the y-axis are 8 meters (twice the device radius) and 70 meters (17.5 times the device radius), respectively. This configuration yields a q factor of 1.528 and an array AEP of 10,098.14 MWh.

(b) Economic Assessment:

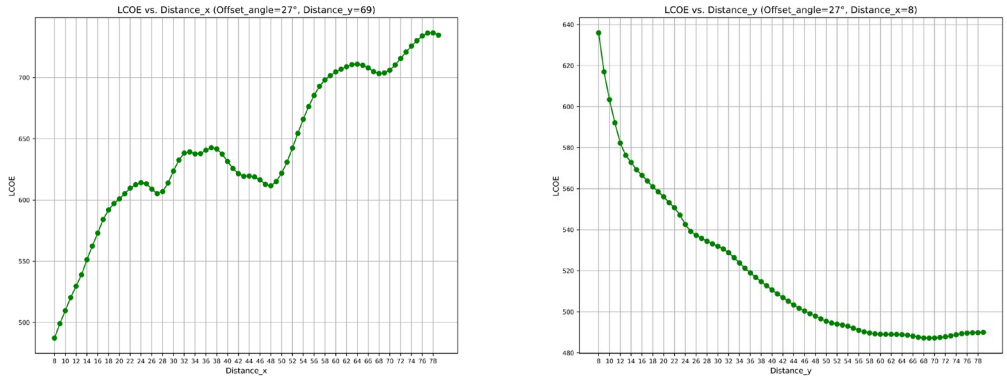

Figure 5.23 LCoE VS Distance in X and Y Axis for Three-row Array @ Real k

During the economic evaluation, an unusual scenario emerged where the technically optimal array configuration diverged from the economically optimal one. In detail, the economically optimal array configuration also featured a rhombus arrangement, with the distance in the x-axis remaining unchanged. However, the distance in the y-axis decreased from 70 meters to 69 meters (equivalent to 17.25 times the device radius). Although this adjustment slightly reduced the AEP from 10,098.14 MWh to 10,097.27 MWh, the LCoE improved to 487.22 EUR/MWh. This improvement is attributed to the reduced in-array cable connection costs resulting from the shortened device spacing.

5.3 Technical and Economic Optimisation under Some Assumptions

In the preceding sections, we delved into the distribution of LCoE and cost distribution of CAPEX under various optimal array configurations, all under the assumption of the current project state and scale being a "small array". This section will alter this assumption by elevating the project state and scale to preliminarily explore whether WEC farms can meet the LCoE target set in the Strategic Energy Technology Plan.

Table 5.5 Distribution of CAPEX for Small Array and High Maturity

Elements	**Three-row Array**	**Three-row Array**	**Three-row Array**
Device Num	10	10	15
State and Scale	Small Array	High Maturity	
Devices	20.5 %	20.5 %	25.3 %
PTO	10.7 %	10.7 %	13.1 %
Mooring or Foundation	5.6 %	5.6 %	6.9 %
Grid Connection	19.5 %	19.5 %	16.6 %
Installation	23.2 %	23.2 %	20.3 %
Decommissioning	20.4 %	20.4 %	17.8 %
Total CAPEX	100 %	100 %	100 %
LCoE	260.19EUR/MWh	171.62EURMWh	168.34EURMWh

We can observe a significant improvement in LCoE as the array state and scale transition from "small array" to "High Maturity", entering the range of 200 EUR/MWh or less, which aligns with the target set by The European strategic energy technology plan for 2025. With the increased number of devices in the array from 10 to 15, the LCoE decreases to 168.34 EUR/MWh.

Chapter 6: Conclusion and Future Works

This thesis commences with exploring current energy policies and renewable energy scenarios, highlighting the wave energy LCoE target set forth by The European Strategic Energy Technology Plan. Subsequently, a wave energy array design tool, based on the MORE-EST Platform from MOREnergy lab, is developed to facilitate the commercialisation of wave energy fields.

Chapter 2 introduces the mathematical models pertinent to the tool, encompassing linear wave theory, point absorber mathematical models, technical models, and economic models.

Chapters 3 to 5 elucidate the development process of the design tool and simulate a WEC array project in the oceans surrounding Italy. The primary process involves project site selection, array generation, and array configuration optimisation. (a) Site selection incorporates three categories of selection criteria: Restrictive Sector, Economic Sector, and Technical Sector criteria. The thresholds for these criteria can be customisable to meet varied marine conditions. (b) Array generation facilitates the creation of arrays at selected sites by users inputting array parameters. (c) Array configuration optimisation employs technical and economic models to quantify interaction effects between devices using q factors and evaluate array economic viability using LCoE to automatically identify optimal configurations under specific wave conditions and WEC parameters.

The selected site in the simulated wave energy project lies west of Sicily, where single-line, two-line, and three-line arrays comprising 10 WECs are generated. Configuration optimisation based on technical and economic factors is conducted for these arrays, resulting in outputs such as q factor against device distance and LCoE against device distance graphs. The rhombus configuration emerges as a relatively superior structure for head sea conditions.

Future work:

(a) Considering the current point absorber approximation may be insufficient under certain conditions, the Boundary Element Method (BEM) for the technical model could be explored.

(b) In the array project simulation, the defined number of devices is 10, a small-scale array. Future work could involve deploying and simulating large-scale arrays.

(c) The design tool developed in this work focuses only on the waters of Italy. In the future, the goal could be expanded to cover the European region or even globally.

References

[1] Communication from the Commission: Energy for the Future: Renewable Sources of Energy White Paper for a Community Strategy and Action Plan. COM (97)599 Final, 26 Nov.1997.

[2] "2020 Climate and Energy Package." Eur-Lex.europa.eu, 19 Sept. 2015, eur-lex.europa.eu/EN/egal-content/summary/2020-climate-and-energy-package.html

[3] "The 2030 Climate and Energy Framework." Europa.eu, European Council, 14 Oct. 2017, www.consilium.europa.eu/en/policies/climate-change/2030-climate-and-energy-framework/.

[4] Paris Agreement to the United Nations Framework Convention on Climate Change, Dec. 12, 2015, T.I.A.S. No. 16-1104.

[5]: European Environment Agency. "European Environment Agency's Home Page." Www.eea.europa.eu, www.eea.europa.eu/en.

[6] European Commission. "The European Green Deal." European Commission, 2020, commission.europa.eu/strategy-and-policy/priorities-2019-2024/european-green-deal_en.

[7] European Council. "Fit for 55." Www.consilium.europa.eu, 2022, www.consilium.europa.eu/en/policies/green-deal/fit-for-55-the-eu-plan-for-a green transition/

[8] "EUR-Lex - 52022DC0108 - EN - EUR-Lex." Europa.eu, 2022, eur-lex.europa.eu/legal content/EN/TXT/?uri=COM%3A2022%3A108%3AFIN.

[9] Dorrell, John, and Keunjae Lee. "The Cost of Wind: Negative Economic Effects of Global Wind Energy Development." Energies, vol. 13, no. 14, 16 July 2020, p. 3667.

[10] "EUR-Lex - 52020DC0741 - EN - EUR-Lex." Europa.eu, 2020, eur-lex.europa.eu/legal content/EN/TXT/?uri=COM%3A2020%3A741%3AFIN.

[11] Edenhofer, O., Pichs-Madruga, R., Sokona, Y., Seyboth, K., Kadner, S., Zwickel, T., ... & Matschoss, P. (Eds.). (2011). Renewable energy sources and climate change mitigation: Special report of the intergovernmental panel on climate change. Cambridge University Press.

[12] Creative Commons (CC) Licenses - Terms." IEA, http://www.iea.org/terms/ creative-commons-cc-licenses.

[13] Bevilacqua, Giovanna, and Barbara Zanuttigh. Overtopping Wave Energy Converters: General Aspects and Stage of Development. 1 Mar. 2011.

[14] Mattiazzo, Giuliana. "State of the Art and Perspectives of Wave Energy in the Mediterranean Sea: Backstage of ISWEC." Frontiers in Energy Research, vol. 7, 29 Oct. 2019.

[15] Eco Wave Power Jaffa Port, Israel,2019, http://ecowavepower.com/israel/.

[16] H24wave - H24 Underwater Wave Energy Converters. http://40southenergy.it.

[17] "Climate Innovation Window - OBREC." Climate Innovation Window, http://www.climateinnovationwindow.eu/innovations/obrec.

[18] IEA-OES. Annual Report: An Overview of Ocean Energy Activities in 2020. http://www.ocean-energy-systems.org/publications/oes-annual-reports/

[19] WAVENERGY.IT S.R.L. Wavenergy.it, http://www.wavenergy.it/about.

[20] Ocean Power Technologies. PB3 PowerBuoy®. http://oceanpowertechnologies .com/pb3-powerbuoy/

[21] BUDAR, K., and J. FALNES. "A Resonant Point Absorber of Ocean-Wave Power." Nature, vol. 256, no. 5517, 1 Aug. 1975, pp. 478–479.

[22] Guo, B. "Point Absorber Wave Energy Converters." Modelling and Optimization of Wave Energy Converters, 131-168, 2022.

[23] Babarit, A. "On the Park Effect in Arrays of Oscillating Wave Energy Converters." Renewable Energy, vol. 58, Oct. 2013, pp. 68–78.

[24] Budal, K. "Theory for Absorption of Wave Power by a System of Interacting Bodies." Journal of Ship Research, vol. 21, no. 04, 1 Dec. 1977, pp. 248–254.

[25] Evans, D. "Some Analytic Results for Two- and Three-Dimensional Wave Energy Absorbers." Power from Sea Waves, 213–248, 1980

[26] McGuinness, Justin, and G. Neil Thomas. Hydrodynamic Optimization of Small Arrays of Heaving Point Absorbers. Vol. 2, no. 4, 13 July 2016, pp. 439–457.

[27] Mavrakos, S.A., and P. Koumoutsakos. "Hydrodynamic Interaction among Vertical Axisymmetric Bodies Restrained in Waves." Applied Ocean Research, vol. 9, no. 3, July 1987, pp. 128–140.

[28] Simon, M J. Multiple Scattering in Arrays of Axisymmetric Wave-Energy Devices. Part 1. A Matrix Method Using a Plane-Wave Approximation. Vol. 120, 1 July 1982, pp. 1–25

[29] Kagemoto, Hiroshi, and Dick K. P. Yue. "Interactions among Multiple Three-Dimensional Bodies in Water Waves: An Exact Algebraic Method." Journal of Fluid Mechanics, vol. 166, no. -1, May 1986, p. 189

[30] J. Cameron McNatt, et al. "A Novel Method for Deriving the Diffraction Transfer Matrix and Its Application to Multi-Body Interactions in Water Waves." Ocean Engineering, vol. 94, 1 Jan. 2015, pp. 173–185

[31] De Chowdhury, S., and R. Manasseh. "Behavior of Eigenmodes of an Array of Oscillating Water Column Devices." Wave Motion, vol. 74, Nov. 2017, pp. 56–72

[32] Göteman, Malin, et al. "Advances and Challenges in Wave Energy Park Optimization—A Review." Frontiers in Energy Research, vol. 8, 6 Mar. 2020.

[33] Babarit, Aurélien. “Impact of Long Separating Distances on the Energy Production of Two Interacting Wave Energy Converters.” Ocean Engineering, vol. 37, no. 8-9, June 2010, pp. 718–729.

[34] Bozzi, Silvia, et al. “Wave Energy Farm Design in Real Wave Climates: The Italian Offshore.” Energy, vol. 122, Mar. 2017, pp. 378–389..

[35] Verbrugghe, Tim, et al. A Comparison Study of a Generic Coupling Methodology for Modeling Wake Effects of Wave Energy Converter Arrays. Vol. 10, no. 11, 25 Oct. 2017, pp. 1697–1697

[36] Thomas, S, et al. “Float Response within an Array: Numerical and Experimental Comparison.” In Proceedings of the 2nd International Conference on Ocean Energy (ICOE), vol. 1517, 1 Jan. 2008.

[37] Weller, S, et al. “Interaction Factors for a Rectangular Array of Heaving Floats in Irregular Waves.” IET Renew. Power Generate., vol. 4: 628–637

[38] Nader, Jean-Roch, et al. “Novel Experimental Modelling of the Hydrodynamic Interactions of Arrays of Wave Energy Converters.” International Journal of Marine Energy, vol. 20, Dec. 2017, pp. 109–124

[39] Bosma, Bret, et al. “Array Modeling and Testing of Fixed OWC Type Wave Energy Converters.” International Marine Energy Journal, vol. 3, no. 3, 4 Dec. 2020, pp. 137–143.

[40] G. Neil Thomas, and D. Gareth Evans. “Arrays of Three-Dimensional Wave-Energy Absorbers.” Journal of Fluid Mechanics, vol. 108: 67–88, 1 July 1981, pp. 67–88

[41] S. A. Mavrakos, and P McIver. “Comparison of Methods for Computing Hydrodynamic Characteristics of Arrays of Wave Power Devices.” Applied Ocean Research, vol. 19, no. 5-6, 1 Oct. 1997, pp. 283–291

[42] McGuinness, Justin, and Gareth Thomas. “Optimization of Wave-Power Arrays without Prescribed Geometry over Incident Wave Angle.” International Marine Energy Journal, vol. 4, no. 1, 25 Mar. 2021, pp. 1–10

[43] McIver, P. “Some Hydrodynamic Aspects of Arrays of Wave-Energy Devices.” Applied Ocean Research, vol. 16, no. 2, Jan. 1994, pp. 61–69.

[44] Thomas Henry Havelock. “Waves due to a Floating Sphere Making Periodic Heaving Oscillations.” Proceedings of the Royal Society of London, vol. 231, no. 1184, 19 July 1955, pp. 1–7.

[45] SET Plan Secretariat SET Plan -Declaration of Intent on Strategic Targets in the Context of an Initiative for Global Leadership in Ocean Energy.

[46] Mendoza, N, et al. “Developing Technology Performance Level Assessments for Early-Stage Wave Energy Converter Technologies (No. NREL/CP-5700-80455).” National Renewable Energy Lab. (NREL), Golden, CO (United States), 2021.

[47] Bastos, Paula, et al. “Life Cycle Assessment of a Wave Energy Device – LiftWEC.” Proceedings of the European Wave and Tidal Energy Conference, vol.

15, 2 Sept. 2023, https://doi.org/10.36688/ewtec-2023-377. Accessed 18 Mar. 2024.

[48] Piscopo, Vincenzo, et al. “Cost-Based Design and Selection of Point Absorber Devices for the Mediterranean Sea.” Energies, vol. 11, no. 4, 16 Apr. 2018, p. 946

[49] Giassi, Marianna, et al. “Economical Layout Optimization of Wave Energy Parks Clustered in Electrical Subsystems.” Applied Ocean Research, vol. 101, 102274, Aug. 2020, p. 102274.

[50] Guanche, R., et al. “A Global Analysis of the Operation and Maintenance Role on the Placing of Wave Energy Farms.” Energy Conversion and Management, vol. 106: 440-456, Dec. 2015, pp. 440–456

[51] Blech, E.M. “Developing a Cost Model for Combined Offshore Farms: The Advantages of Co-Located Wind and Wave Energy.” Master’s Thesis, Universitat Politècnica de Catalunya, 2023.

[52] Astariz, S., and G. Iglesias. “The Economics of Wave Energy: A Review.” Renewable and Sustainable Energy Reviews, vol. 45: 397-408, May 2015, pp. 397–408.

[53] Johanning, L, et al. “Mooring Design Approach for Wave Energy Converters.” Proceedings of the Institution of Mechanical Engineers, Part M: Journal of Engineering for the Maritime Environment, vol. 220, no. 4, 1 Dec. 2006, pp. 159–174.

[54] Herbert-Acero, José, et al. “A Review of Methodological Approaches for the Design and Optimization of Wind Farms.” Energies, vol. 7, no. 11, 29 Oct. 2014, pp. 6930–7016.

[55] Victor R.J.H. Timmers, et al. “All-DC Offshore Wind Farms: When Are They More Cost-Effective than AC Designs?” IET Renewable Power Generation, vol. 17, no. 10, 17 July 2022, pp. 2458–2470.

[56] Corrales-Gonzalez, Manuel, et al. “Feasibility of Wave Energy Harvesting in the Ligurian Sea, Italy.” Sustainability, vol. 15, no. 11, 5 June 2023, pp. 9113–9113.

[57] A Horizon 2020 Project Developing a Lift-Based Wave Energy Converter. http://liftwec.com/.

[58] Pennock, Shona, et al. “Deriving Current Cost Requirements from Future Targets: Case Studies for Emerging Offshore Renewable Energy Technologies.” Energies, vol. 15, no. 5, 25 Feb. 2022, pp. 1732–1732.

[59] Sverdrup, H.U., and W.H. Munk. “Wind, Sea and Swell: Theory of Relations for Forecasting (No. 601).” Hydrographic Office, 1947.

[60] Hasselmann, Klaus. “On the Non-Linear Energy Transfer in a Gravity-Wave Spectrum Part 1. General Theory.” Journal of Fluid Mechanics, vol. 12, no. 04, 1 Apr. 1962, pp. 481–500.

[61] Hasselmann, Klaus. “On the Spectral Dissipation of Ocean Waves due to White Capping.” Boundary-Layer Meteorology, vol. 6, no. 1-2, Mar. 1974, pp. 107–127.

[62] Hasselmann, S., et al. “Computations and Parameterizations of the Nonlinear Energy Transfer in a Gravity-Wave Spectrum. Part II: Parameterizations of the Nonlinear Energy Transfer for Application in Wave Models.” Journal of Physical Oceanography, vol. 15, no. 11, Nov. 1985, pp. 1378–1391.

[63] Cavaleri, Luigi, et al. “Wind–Wave Modeling: Where We Are, Where to Go.” Journal of Marine Science and Engineering, vol. 8, no. 4, 7 Apr. 2020, p. 260.

[64] Weiss, Carlos V.C., et al. “Marine Renewable Energy Potential: A Global Perspective for Offshore Wind and Wave Exploitation.” Energy Conversion and Management, vol. 177: 43-54, Dec. 2018, pp. 43–54.

[65] Maldonado, Ana D., et al. “A Bayesian Network Model to Identify Suitable Areas for Offshore Wave Energy Farms, in the Framework of Ecosystem Approach to Marine Spatial Planning.” Science of the Total Environment, vol. 838, Sept. 2022, p. 156037

[66] Kaldellis, J, et al. “Wave Energy Exploitation in the North Aegean Sea: Spatial Planning of Potential Wave Power Stations.” In Proceedings of the 15th International Conference on Environmental Science and Technology, Rhodes, Greece, vol. 31, 2017.

[67] Hiles, Clayton, et al. “Wave Energy Converter Annual Energy Production Uncertainty Using Simulations.” Journal of Marine Science and Engineering, vol. 4, no. 3, 2 Sept. 2016, p. 53

[68] Monteiro, L, et al. Statistical Analysis of Wave Energy Resources Available for Conversion at Natural Caves of Cape-Verde Islands. 20 Jan. 2016

[69] Flocard, Francois, et al. “Multi-Criteria Evaluation of Wave Energy Projects on the South-East Australian Coast.” Renewable Energy, vol. 99, Dec. 2016, pp. 80–94

[70] Cervelli, Giulia, et al. Wave and Wind RES Platform Database and Algorithms Description. 10 Oct. 2022

[71] Arinaga, Randi A., and Kwok Fai Cheung. “Atlas of Global Wave Energy from 10 Years of Reanalysis and Hindcast Data.” Renewable Energy, vol. 39, no. 1, Mar. 2012, pp. 49–64.

[72] Folley, M., and T.J.T. Whittaker. “Analysis of the Nearshore Wave Energy Resource.” Renewable Energy, vol. 34, no. 7, July 2009, pp. 1709–1715

[73] Sanil Kumar, V., and T.R. Anoop. “Wave Energy Resource Assessment for the Indian Shelf Seas.” Renewable Energy, vol. 76, Apr. 2015, pp. 212–219

[74] Lavidas, George. “Selection Index for Wave Energy Deployments (SIWED): A Near-Deterministic Index for Wave Energy Converters.” Energy, vol. 196, Apr. 2020, p. 117131.

[75] Weiss, Carlos V.C., et al. “Marine Renewable Energy Potential: A Global Perspective for Offshore Wind and Wave Exploitation.” Energy Conversion and Management, vol. 177, Dec. 2018, pp. 43–54.

[76] Abaei, Mohammad Mahdi, et al. “Developing a Novel Risk-Based Methodology for Multi-Criteria Decision Making in Marine Renewable Energy Applications.” Renewable Energy, vol. 102, Mar. 2017, pp. 341–348

[77] “Natural Earth.” Natural Earth, http://www.naturalearthdata.com/

[78] “Marine Regions.” Www.marineregions.org, http://www.marineregions.org/

[79] EMODnet Human Activities, Cables, Power, Actual Routes (europa.eu)

https://ows.emodnet-humanactivities.eu/geonetwork/srv/api/records/41b339f8-b29c-4550-b787-3d68f08fdbcc

[80] EMODnet Human Activities, Pipelines.” EMODnet Human Activities, http://ows.emodnet-humanactivities.eu/geonetwork/srv/api/records/aca3dd01-77ac-47fe-8291-6ca916daaa6d.

[81] “EMODnet Human Activities, Military Areas.” EMODnet Human Activities, http://ows.emodnet-humanactivities.eu/geonetwork/srv/api/records/579e4a3b-95e4-48c6-8352-914ebae0ae1d

[82] “EMODnet Human Activities, Environment, Common Database on Designated Areas (CDDA).” EMODnet Human Activities, http://ows.emodnet-humanactivities.eu/geonetwork/srv/api/records/3362d8b1-a12e-4d1d-a0d8-1834e9db00f3

[83] “EMODnet Human Activities, Oil and Gas, Active Licenses.” EMODnet Human Activities, http://ows.emodnet-humanactivities.eu/geonetwork/srv/api/records/d9da64ae-4bff-4cae-9ee8-58d9acc1d0f

[84] “EMODnet Human Activities.” EMODnet Human Activities, 3 Aug. 2022, http://emodnet.ec.europa.eu/en/human-activities.

[85] “EMODnet Human Activities, Vessel Density Map.” EMODnet Human Activities, http://ows.emodnet-humanactivities.eu/geonetwork/srv/api/records/0f2f3ff1-30ef-49e1-96e7-8ca78d58a07c

[86] “Download Grid Maps.” www.entso e.eu/data/map/downloads/.

[87] “Gridded Bathymetry Data (General Bathymetric Chart of the Oceans).” GEBCO, http://www.gebco.net/data_and_products/gridded_bathymetry_data/.

[88] “Map of the Week - Seabed Substrates.” European Marine Observation and Data Network (EMODnet), 17 Dec. 2021, http://emodnet.ec.europa.eu/en/map-week-%E2%80%93-seabed-substrates.

[89] O’Connell, Ross, et al. “Development and Application of a GIS for Identifying Areas for Ocean Energy Deployment in Irish and Western UK

Waters." Journal of Marine Science and Engineering, vol. 11, no. 4, 13 Apr. 2023, pp. 826–826.

[90] R.R., Williams III. "Suitability Analysis for Wave Energy Farms off the Coast of Southern California: An Integrated Site Selection Methodology." Doctoral Dissertation, University of Southern California, 2018.

[91] Kaldellis, J, et al. "Wave Energy Exploitation in the North Aegean Sea: Spatial Planning of Potential Wave Power Stations." In Proceedings of the 15th International Conference on Environmental Science and Technology, Rhodes, Greece, vol. 31, 2017.

[92] Vasileiou, Margarita, et al. "GIS-Based Multi-Criteria Decision Analysis for Site Selection of Hybrid Offshore Wind and Wave Energy Systems in Greece." Renewable and Sustainable Energy Reviews, vol. 73, June 2017, pp. 745–757

[93] Ophelie Choupin, et al. "Integration of Assessment-Methods for Wave Renewable Energy: Resource and Installation Feasibility." Renewable Energy, vol. 185: 455-482, 1 Feb. 2022, pp. 455–482

[94] Monteiro, L, et al. "Statistical Analysis of Wave Energy Resources Available for Conversion at Natural Caves of Cape-Verde Islands." Ocean Science Discussions, vol. 1-23, 20 Jan. 2016.

[95] Ricci, Pierpaolo, et al. Point-Absorber Arrays: A Configuration Study off the Portuguese West-Coast. 1 July 2007.

[96] Engström, J., et al. "Performance of Large Arrays of Point Absorbing Direct-Driven Wave Energy Converters." Journal of Applied Physics, vol. 114, no. 20, 28 Nov. 2013, p. 204502.

[97] Faraggiana, Emilio, et al. "Influence of Directional Wave Spreading on a WEC Device." International Marine Energy Journal, vol. 5: 227, no. 2, 30 Sept. 2022, pp. 227–242

[98] Sinha, Ashank, et al. "Performance of Optimally Tuned Arrays of Heaving Point Absorbers." Renewable Energy, vol. 92: 517-531, July 2016, pp. 517–531

[99] Fitzgerald, C, and G Thomas. "A Preliminary Study on the Optimal Formation of an Array of Wave Power Devices." In Proceedings of the 7th European Wave and Tidal Energy Conference, Porto, Portugal (Pp. 11-14), Sept. 2007.

[100] Göteman, Malin, et al. "Optimizing Wave Energy Parks with over 1000 Interacting Point-Absorbers Using an Approximate Analytical Method." International Journal of Marine Energy, vol. 10, no. 113126, June 2015, pp. 113–126

Appendix

A1 Code Example

This part of the Appendix section indicates some code examples for this thesis work used in Python.

A1.1 Example of "Buffer Function" Code (Section 3.4)

```
# This code is to build a Buffered region for Pipelines
# The Buffer Distance is set as 500 meters.

import geopandas as gpd
import matplotlib.pyplot as plt
import os

# Get the directory of the current script
script_directory = os.path.dirname(os.path.abspath(__file__))

# Set the input folder name
input_folder_name = "raw_Pipeline_shp"

# Create the input folder path
input_folder_path = os.path.join(script_directory, input_folder_name)

# Set the shapefile path within the input folder
shapefile_path = os.path.join(input_folder_path, "pipelinesLine.shp")
data = gpd.read_file(shapefile_path)

# Set the buffer distance @500 meters
buffer_distance = 500

# Re-project the .shp file to a projected CRS
data = data.to_crs("EPSG:32633")

# Create a buffer region by buffer function
buffered_data = data.buffer(buffer_distance)


# Set the output folder name
output_folder_name = "buffer_Pipeline_shp"

# Create the output folder path
output_folder_path = os.path.join(script_directory, output_folder_name)

# Create the output folder if it doesn't exist
if not os.path.exists(output_folder_path):
    os.makedirs(output_folder_path)

# Set the output shapefile path within the output folder
output_shapefile_path = os.path.join(output_folder_path, "buffered_data.shp")

# Save the buffered data as a new shapefile
buffered_data.to_file(output_shapefile_path)
```

```
# Create a plot to show the buffered region
fig, ax = plt.subplots(figsize=(10, 10))

# Plot the original region
# data.plot(ax=ax, color='blue')

# Plot the buffered region
buffered_data.plot(ax=ax, color='red')

# Set plot title and labels
ax.set_title("Buffered Region@500m")
ax.set_xlabel("X")
ax.set_ylabel("Y")

# Display the plot
plt.show()
```

A1.2 Example of "Vessel Density Quantification" Code(Section 3.4)

```
import rasterio
import numpy as np
import matplotlib.pyplot as plt
from matplotlib.colors import ListedColormap

# Open the file
file_path = r"C:\Users\yuwei\Desktop\Database\Economic
Sector\EMODnet_HA_Vessel_Density_all_2017-2022Avg\EMODnet_Vessel_Density_17-
22\vesseldensity_all_2022.tif"
with rasterio.open(file_path) as src:
    # Read the raster data
    array = src.read(1)
    # Get the geotransform and crs information
    transform = src.transform
    crs = src.crs

# Mask values less than or equal to 0 in the original array
mask = array < 0
array[mask] = 0

# Define a new classification scheme
class_bounds = [0, 0.187, 0.585, 15.963, float('inf')]

# Initialize an array of zeros with the same shape as the original data
array_classified = np.zeros_like(array)

# Classify the data
for i, bounds in enumerate(zip(class_bounds[:-1], class_bounds[1:]), start=1):
    array_classified[(array > bounds[0]) & (array <= bounds[1])] = i

# Save the classified array to a new GeoTIFF file
output_file_path = r"C:\Users\yuwei\Desktop\Afterprocess\Economical Sector\Vessel
density2022\vesseldensity2022.tif"
with rasterio.open(output_file_path, 'w', driver='GTiff', height=array_classified.shape[0],
                   width=array_classified.shape[1], count=1, dtype=array_classified.dtype,
                   crs=crs, transform=transform) as dst:
    dst.write(array_classified, 1)
```

```
# Define colors
color_dict = {0: 'none',  # Transparent
              1: 'yellow',
              2: 'darkorange',
              3: 'brown',
              4: 'black'}

# Create a colormap from the dictionary
cmap = ListedColormap([color_dict[i] for i in sorted(color_dict.keys())])

# Create a new figure
fig, ax = plt.subplots(figsize=(10, 10), dpi=600)

# Plot the classified data with its original resolution
img = ax.imshow(array_classified, cmap=cmap)

# Display the plot
plt.show()
```

A1.3 Example of "Mask function" Code(Section 3.4)

```
import xarray as xr
import matplotlib.pyplot as plt
import cartopy.crs as ccrs
import cartopy.feature as cfeature
import cartopy.io.shapereader as shpreader
import geopandas as gpd

# Open the datasets and load the variables
data1 = xr.open_dataset(r'C:\Users\yuwei\Desktop\Afterprocess\Technical
Sector\wave_power\10to20_mean\final_mean_Wave_Power.nc')
wave_power_mask = data1['10to20_mean_Wave_Power_masked']
data2 = xr.open_dataset(r'C:\Users\yuwei\Desktop\Afterprocess\Technical
Sector\swh\10to20_mean\10to20_swh.nc')
swh_mask = data2['10to20_mean_swh_masked']
data3 = xr.open_dataset(r'C:\Users\yuwei\Desktop\Afterprocess\Technical
Sector\MVI\wave2020_MVI.nc')
mvi_mask = data3['MVI_mask']
data4 = xr.open_dataset(r'C:\Users\yuwei\Desktop\Afterprocess\Technical
Sector\Accessibility\Accessibility@2010to2020.nc')
accessibility_mask = data4['Accessibility_Frequency']
data5 = xr.open_dataset(r'C:\Users\yuwei\Desktop\Afterprocess\Technical
Sector\Bathymetry\Bathymetry.nc')
data5 = data5.rename({'lon': 'longitude', 'lat': 'latitude'})
bathymetry_mask = data5['region_int']

bathymetry_mask_bool = bathymetry_mask != 0.0

# Interpolate all the other datasets to match bathymetry_mask
wave_power_mask_interpolated = wave_power_mask.interp(
  latitude=bathymetry_mask.latitude,
  longitude=bathymetry_mask.longitude
)
swh_mask_interpolated = swh_mask.interp(
  latitude=bathymetry_mask.latitude,
  longitude=bathymetry_mask.longitude
)
mvi_mask_interpolated = mvi_mask.interp(
```

```
    latitude=bathymetry_mask.latitude,
    longitude=bathymetry_mask.longitude
)
accessibility_mask_interpolated = accessibility_mask.interp(
    latitude=bathymetry_mask.latitude,
    longitude=bathymetry_mask.longitude
)

# Convert to boolean masks
wave_power_mask_bool_resampled = wave_power_mask_interpolated > 0
swh_mask_bool_resampled = swh_mask_interpolated > 0
mvi_mask_bool_resampled = mvi_mask_interpolated > 0
accessibility_mask_bool_resampled = accessibility_mask_interpolated >= 0.6

# Combine the masks
combined_mask_resampled = (wave_power_mask_bool_resampled
                           & swh_mask_bool_resampled
                           & mvi_mask_bool_resampled
                           & accessibility_mask_bool_resampled
                           & bathymetry_mask_bool)

# Convert the wave power data to a masked array using the resampled mask
wave_power_data_resampled =
wave_power_mask_interpolated.where(combined_mask_resampled)

# Save to a new netCDF file    #### unuseful
# wave_power_data_resampled.to_netcdf(r'C:\Users\yuwei\Desktop\Afterprocess\Technical
Sector\Final area\final_area inPower @T,R.nc')

# Open the mwd dataset
data6 = xr.open_dataset(r'C:\Users\yuwei\Desktop\Afterprocess\Technical
Sector\mwd\10to20_mean\10to20_mwd.nc')
mwd_mask = data6['10to20_mean_mwd']

# Interpolate the mwd dataset to match bathymetry_mask
mwd_mask_interpolated = mwd_mask.interp(
    latitude=bathymetry_mask.latitude,
    longitude=bathymetry_mask.longitude
)

# Mask the mwd data using the combined mask
mwd_data_resampled = mwd_mask_interpolated.where(combined_mask_resampled)

# Save to a new netCDF file #### unuseful
# mwd_data_resampled.to_netcdf(r'C:\Users\yuwei\Desktop\Afterprocess\Technical
Sector\Final area\final_area inmwd @T,R.nc')

# Create a new figure
fig = plt.figure(figsize=(15, 15), dpi=900)

# Create a GeoAxes in the tile's projection.
ax = plt.axes(projection=ccrs.PlateCarree())


# Load the forbidden area shapefiles
shp_files = [
    r'C:\Users\yuwei\Desktop\Afterprocess\Restricted Sector\Power
Cables_buffer@500m\buffered_data.shp',
    r'C:\Users\yuwei\Desktop\Afterprocess\Restricted
```

```
Sector\Pipeline_buffer@500m\buffered_data.shp',
    r'C:\Users\yuwei\Desktop\Afterprocess\Restricted Sector\Active
licences_buffer@500m\buffered_data.shp',
    r'C:\Users\yuwei\Desktop\Database\Restricted Sector\Natura 2000
sites\natura2000areas.shp',
    r'C:\Users\yuwei\Desktop\Database\Restricted Sector\Nationally Designated
Areas\cddaareas.shp',
    r'C:\Users\yuwei\Desktop\Database\Restricted Sector\Military Areas
(Polygons)\militaryareaspolyPolygon.shp'
]

for shp_file in shp_files:
    gdf = gpd.read_file(shp_file)
    gdf = gdf.cx[-20:45, 30:47]  # Crop by given latitude and longitude
    ax.add_geometries(gdf.geometry, ccrs.PlateCarree(), facecolor='white', edgecolor='none',
alpha=1)

# Plot the mwd data
plt.contourf(mwd_data_resampled.longitude, mwd_data_resampled.latitude,
mwd_data_resampled, transform=ccrs.PlateCarree())

# Add a colorbar
plt.colorbar(label='10to20_mean_mwd')

# Set the map extent
ax.set_extent([mwd_data_resampled.longitude.min(), mwd_data_resampled.longitude.max(),
mwd_data_resampled.latitude.min(), mwd_data_resampled.latitude.max()])


# Add the eez feature to the map
eez = shpreader.Reader(r'C:\Users\yuwei\Desktop\Database\Basemap\Exclusive Economic
Zone\eez.shp')
ax.add_geometries(eez.geometries(), ccrs.PlateCarree(), edgecolor='red', facecolor='none')

# Load the coastline shapefile
coastlines =
shpreader.Reader(r'C:\Users\yuwei\Desktop\Database\Coastlines\ne_10m_coastline\ne_10m_c
oastline.shp')
ax.add_geometries(coastlines.geometries(), ccrs.PlateCarree(), edgecolor='black',
facecolor='none')

plt.title('Masked MWD')
plt.xlabel('Longitude')
plt.ylabel('Latitude')

# Save the figure
plt.savefig('Masked_MWD.png')
```

A1.4 Example of “Sensitivity Analysis” Code(Section 3.5)

```
import xarray as xr
import numpy as np
import matplotlib.pyplot as plt
import cartopy.crs as ccrs

# Define the scale factor and Base_Condition threshold
scale_factor = 0.7  # 30% stricter
BC_down_limit = 0.5
```

```
BC_up_limit = 4

# Full path to the folder containing the files
folder_path = r'C:\Users\yuwei\Desktop\Afterprocess\Technical Sector\swh\year_mean\\'

# Step 1: List all .nc files
file_paths = [f'{folder_path}mean_swh_{i}_test.nc' for i in range(2010, 2020)]

# Step 2: Open and combine all .nc files
datasets = [xr.open_dataset(fp) for fp in file_paths]
combined_data = xr.concat(datasets, dim='time')

# Step 3: Calculate the final mean swh
final_mean_swh = combined_data['mean_swh'].mean(dim='time')

# Step 4: Create a new array for values which meet the condition
values_masked = np.where((final_mean_swh >= (2-scale_factor)*BC_down_limit) &
(final_mean_swh <= scale_factor*BC_up_limit), final_mean_swh, np.nan)

# Step 5: Add the new array to the dataset
final_mean_swh_dataset = final_mean_swh.to_dataset(name='10to20_mean_swh')
final_mean_swh_dataset['10to20_mean_swh_masked'] = xr.DataArray(values_masked,
coords=final_mean_swh.coords)

# Step 6: Write the final Dataset to a .nc file
final_mean_swh_dataset.to_netcdf(r'C:\Users\yuwei\Desktop\Sensitivity
analysis\swh_stricter\10to20_swh_stricter@30%.nc')

# Step 7: Extract the necessary data for plotting
latitude = final_mean_swh_dataset['latitude']
longitude = final_mean_swh_dataset['longitude']
values = final_mean_swh_dataset['10to20_mean_swh_masked'].values

# Step 8: Plot the mean data using matplotlib and cartopy
fig = plt.figure(figsize=(10, 10),dpi=600)
ax = plt.axes(projection=ccrs.PlateCarree())

# specify the levels for colorbar
levels = np.linspace((2-scale_factor)*BC_down_limit, scale_factor*BC_up_limit, 21)

plt.contourf(longitude, latitude, values, levels=levels, transform=ccrs.PlateCarree())
ax.coastlines()

plt.colorbar()

plt.title('Mean significant wave height @2010to2020')
plt.xlabel('Longitude')
plt.ylabel('Latitude')

# Save the figure instead of showing it
plt.savefig('2010to2020_mean_swh.png')
```

A1.5 Example of "Wave Parameter Calculation" Code

```
# This code is a pre-code for q_factor calculation, and it is used to calculate some wave
paramenters that are used in the q_factor calculation.
# This wave datasets are the 'Dati Onde' datasets from Prof. Faraggiana.
# IN THIS CODE, the wave number k computed is a fixed value.
```

```
import numpy as np
from netCDF4 import Dataset
import os

def read_wave_data(target_longitude, target_latitude, data_path):
    """
    Read wave data from NetCDF files and extract significant wave height (SWH) and mean wave period (MWP) data.

    Input Parameters:
    - target_longitude: Longitude of the target location.
    - target_latitude: Latitude of the target location.
    - data_path: Path to the directory containing wave data files.

    Returns:
    - swh_mean: Mean significant wave height.
    - mwp_mean: Mean mean wave period.
    """
    # Initialize a list to store swh and mwp arrays
    swh_list = []
    mwp_list = []

    # Read data and extract swh and mwp data
    for year in range(2010, 2020):
        file_path = f"{data_path}\\wave{year}.nc"
        with Dataset(file_path, 'r') as nc_file:

            longitudes = np.array(nc_file.variables['longitude'][:])  # Extract longitudes
            latitudes = np.array(nc_file.variables['latitude'][:])    # Extract longitudes

            # Find the nearest longitude and latitude indices to the target location
            lon_index = (np.abs(longitudes - target_longitude)).argmin()
            lat_index = (np.abs(latitudes - target_latitude)).argmin()

            # Input the swh and mwp data @ target location and append to mwp_data list
            swh_list.extend(np.array(nc_file.variables['swh'][:, lat_index, lon_index]))
            mwp_list.extend(np.array(nc_file.variables['mwp'][:, lat_index, lon_index]))

    # calculate the mean swh and mean mwp
    swh_mean = np.mean(swh_list)
    mwp_mean = np.mean(mwp_list)

    # Overwrite swh_mean and mwp_mean to make programme calculate
    # the wave number @ a given condition, eg: most occurrence condition
    # swh_mean = 0.375  # For check
    # mwp_mean = 3.125  # For check

    return swh_mean, mwp_mean


def compute_wave_properties(mwp, h, decimal_places=3):
    """
        Compute wave properties such as wave number (k) and water depth type based on the mean wave period (mwp).

        Input Parameters:
        - mwp: mean wave period.
        - h: Water depth. [m]
```

```
    - decimal_places

    Returns:
    - k: Wave number.
    - depth_type: Type of water depth.
    """
    g = 9.81  # Gravitational acceleration
    T = mwp   # Mean wave period

    # Calculate wavelength
    lamb = g / (2 * np.pi) * T ** 2

    # Calculate angular frequency
    omega = 2 * np.pi / T

    # Determine the depth condition
    h_lambda_ratio = abs(h) / lamb
    if h_lambda_ratio > 0.5:
        # Deep water
        depth_type = "Deep water"
        k = omega ** 2 / g
    elif h_lambda_ratio < 0.05:
        # Shallow water
        depth_type = "Shallow water"
        k = np.sqrt(omega ** 2 / (g * abs(h)))
    else:
        # Intermediate water
        depth_type = "Intermediate water"
        k = brute_force_k_search(omega, h)

    # Round the value of k to the specified decimal places
    k = round(k, decimal_places)

    return k, depth_type, lamb, omega

def brute_force_k_search(omega, h, step=0.0001, k_min=0.000, k_max=5.000):
    """
    Perform a brute-force search to find the wave number (k) that satisfies the dispersion relation.

    Input Parameters:
    - omega: Angular frequency.
    - h: Water depth.
    - step: Step size for the search.
    - k_min: Minimum value of k to search.
    - k_max: Maximum value of k to search.

    Returns:
    - best_k: Optimal wave number that satisfies the dispersion relation.
    """
    # Parameters definition and Initialization
    best_k = k_min
    min_diff = float('inf')

    # Iterate over the range of wave numbers to find the optimal k
    for k in np.arange(k_min, k_max + step, step):
        # Calculate the difference between the calculated and expected angular frequency
        diff = abs(dispersion_relation(k, omega, h))

        if diff < min_diff:
```

```
            min_diff = diff
            best_k = k

    return best_k

def dispersion_relation(k, omega, h):
    """
        Compute the dispersion relation for a given wave number (k), angular frequency (omega), and
water depth (h).

        Input Parameters:
        - k: Wave number.
        - omega: Angular frequency.
        - h: Water depth.

        """
    g = 9.81  # gravitational acceleration
    return omega ** 2 - g * k * np.tanh(k * abs(h))


######################################### Inputs
##########################################
# Get the directory of the current script
script_directory = os.path.dirname(os.path.abspath(__file__))

# Set the input folder name
input_folder_name = "Dati Onde"

data_path = os.path.join(script_directory, input_folder_name)

# Geo Information
target_longitude = 11.5
target_latitude = 38
h = -100  # water depth meter

# Read wave data and calculate mean swh and mean mwp, via function
swh_mean, mwp_mean = read_wave_data(target_longitude, target_latitude, data_path)

print(f"Mean SWH: {swh_mean:.2f} meters")
print(f"Mean MWP: {mwp_mean:.2f} seconds")

# Compute wave properties based on mean mwp and water depth
k, depth_type, lamb, omega = compute_wave_properties(mwp_mean, h)
print(f"Estimated wave length (λ): {lamb:.2f} meters")
print(f"Wave number (k): {k} rad/m")
print(f"Angular frequency (ω): {omega:.5f} rad/s")
print(f"Water depth type: {depth_type}")
```